RESEARCH ARTICLE

Key Points:
- We describe fjord and shelf circulation patterns in two large glacial fjords
- Time-dependent, externally driven intermediary circulation dominates both fjords
- We charactertize these fjords in estuarine parameter space

Supporting Information:
- Readme file
- Supporting table
- Supporting figures

Correspondence to:
D. A. Sutherland,
dsuth@uoregon.edu

Characteristics and dynamics of two major Greenland glacial fjords

David A. Sutherland[1], Fiammetta Straneo[2], and Robert S. Pickart[2]

[1]Department of Geological Sciences, University of Oregon, Eugene, Oregon, USA, [2]Department of Physical Oceanography, Woods Hole Oceanographic Institution, Woods Hole, Massachusetts, USA

Abstract The circulation regimes of two major outlet glacial fjords in southeastern Greenland, Sermilik Fjord (SF) and Kangerdlugssuaq Fjord (KF), are investigated using data collected in summer 2009. The two fjords show similar flow patterns, with a time-dependent, vertically sheared flow structure dominating over the background estuarine flow driven by buoyancy input. We show that this time-dependent flow is consistent with circulation induced by density interface fluctuations at the fjord mouth, often referred to as intermediary circulation. One difference between the fjords is that the hydrographic and velocity structure below a surface modified layer is found to be three layer in KF in summer, compared to two layer in SF. Outside each fjord, large-scale geostrophic currents dictate the stratification at the mouth, although the way in which these large-scale flows impinge on each fjord is distinct. Combining the observations with estimates from existing theories, we find the magnitudes of the estuarine (Q_e) and intermediary (Q_i) circulation and show that $Q_i >> Q_e$, although along-fjord winds can also be significant. We expect that the critical parameter determining Q_i/Q_e is the sill depth compared to the fjord depth, with shallower sills corresponding to weaker intermediary circulation. Finally, we discuss the implications of strong intermediary circulation on calculating heat transport to the glacier face and its potential feedbacks on the background circulation in these highly stratified estuaries.

1. Introduction

Greenland's fjords act as important connections between the outlet glaciers that drain the Greenland Ice Sheet (GrIS) and the oceanic boundary currents of the subpolar and Arctic Seas that surround the continent. From an oceanographers' point of view, the fjords act as estuaries, mixing zones that transform and export the submarine melt and runoff from the GrIS onto the shelf, potentially affecting the shelf circulation [e.g., *Yankovsky and Chapman*, 1997; *Hickey and Banas*, 2003; *Murray et al.*, 2010]. From a glaciologists' perspective, the fjords are mixing zones as well, but the relevant flow in this case is that which transports heat directly to the glacier face, setting the submarine melt rate [*Jenkins*, 1999; *Sciascia et al.*, 2013] and mechanically forcing any solid ice acting as a buttress to the glacier (including ice mélange and sea ice) [*Amundson et al.*, 2010]. These two views of fjord circulation share a common dynamical framework. A buoyancy-driven estuarine exchange flow drives a net circulation in the fjord that outputs fresher water and draws in saltier seawater, with the magnitude set by the initial buoyancy input and the rate of entrainment [e.g., *MacCready and Geyer*, 2010; *Stigebrandt*, 2012; *Motyka et al.*, 2003]. However, in Greenland's large glacial fjords, other mechanisms can drive significant circulation that may overwhelm any estuarine signal and potentially affect the total amount of heat that reaches the glacier face. These mechanisms include the time-dependent intermediary circulation (often called geostrophic control) forced by density variations in the coastal water at the fjord mouth [e.g., *Klinck et al.*, 1981; *Stigebrandt*, 1990; *Nilsen et al.*, 2008; *Straneo et al.*, 2010; *Jackson et al.*, 2014], tidal residual flow [*Ianniello*, 1977; *Winant*, 2008], and local wind-driven flow [e.g., *Svendsen and Thompson*, 1978; *Klinck et al.*, 1981]. In Sermilik Fjord, for example, *Straneo et al.* [2010] observed that a two-layer intermediary circulation dominated the velocity variability, with a characteristic time scale of 3–6 days (this time scale is referred to throughout as synoptic scale, due to its relation to weather systems). Progress in untangling fjord circulation must be made to understand which mechanisms, if any, are responsible for the connections observed between warm subsurface ocean waters and outlet glacier acceleration [e.g., *Holland et al.*, 2008].

Adding to the complexity of these different mechanisms is the observation that the estuarine exchange flow can have multiple cells, i.e., it is not restricted to only a surface outflow and deep inflow. In Sermilik

Fjord, *Straneo et al.* [2011] used hydrographic anomalies to show two regions of outflow, one at the surface, and one at the interface depth between the dominant two-layer stratification. This multicell circulation has recently been confirmed in numerical modeling studies simulating the buoyancy-driven (by subglacial discharge and submarine melting) circulation in an idealized "Sermilik Fjord" [*Sciascia et al.*, 2013].

Another important factor influencing the fjord circulation involves the release of surface melt at the base of the glacier ("subglacial discharge")—a highly seasonal process. Recent theoretical and modeling studies suggest that in summer subglacial discharge is the dominant buoyancy forcing (i.e., much larger than submarine melting) [*Jenkins*, 1999; *Sciascia et al.*, 2013; *Xu et al.*, 2012].

Given the complex, time variable circulation observed in Greenland's large fjords, as well as the cost and difficulty of obtaining these measurements, it is of interest to know *a priori* what mechanisms might control the circulation in a given fjord. For example, where and when does the externally driven intermediary circulation dominate over the glacier-driven, estuarine exchange flow? What sets the water properties that reach the mouth of these fjords? How often are measurements needed to determine the heat transport at the glacier face, i.e., how long of a time average is necessary to resolve the net exchange of heat? These questions are difficult to answer for any fjord at present, nor do we even know if individual glacial fjords in Greenland will respond differently to the same external forcing.

The goal of this study is to examine two systems in SE Greenland in order to begin to build the parameter space needed to explore the possible mechanisms controlling fjord circulation around Greenland. To accomplish this goal, we use a spatially well-resolved ship-based survey of two large glacial fjords in Greenland to characterize the important circulation regimes and dynamics that govern them. We focus on the summer regime, i.e., when there is active subglacial discharge, because our sections are limited to summer surveys. We show evidence that supports the observation that the water properties and flow inside these fjords are variable on short, synoptic time scales, in agreement with the intermediary circulation theory. At the mouth of each fjord, we find a geostrophic regime that is governed by the large-scale boundary current dynamics of the subpolar gyre. The outflow from the fjords, however, is not small and may potentially be an important part of the freshwater and volume budget of the subpolar gyre. Finally, we use simple theoretical ideas to predict the magnitude of the intermediary and estuarine circulation in these two fjords and discuss what parameters are needed to extend these predictions to other fjord systems.

2. Data

2.1. Physical Setting

Sermilik Fjord (SF) and Kangerdlugssuaq Fjord (KF) connect the GrIS to the Irminger Sea (Figure 1). Figure 1 shows the bathymetry for the region and fjords, indicating these are both deep-silled fjords, with the actual shallowest sills located near the shelf break of the Irminger Sea [*Sutherland et al.*, 2013]. For SF, Helheim Glacier flows into 20 km long Helheim Fjord, a side fjord that, in turn, connects to SF, an ∼80 km long, ∼6 km wide fjord that runs 16° east of north (Figures 1 and 2). A relatively narrow and deep channel runs perpendicular to the mouth of SF with a maximum depth of 650 m and width of ∼8 km. This channel stems from a major shelf trough that cuts a sinuous path toward SF and appears to continue westward, although the bathymetric data are too scarce in this area to confirm this.

Farther north, Kangerdlugssuaq Glacier empties into KF, a ∼70 km fjord that runs 340° east of north, with a maximum depth of ∼900 m and average width of 6 km. Another major trough, the Kangerdlugssuaq Trough, runs from the shelf break to the mouth of KF.

Helheim Glacier and Kangerdlugssuaq Glacier are both large outlet glaciers with sizable ice fluxes even by GrIS standards (fifth and second out of the entire GrIS in a recent study) [*Enderlin et al.*, 2014], with near vertical calving faces ∼600 m deep and 5–6 km wide. Both glaciers retreated and accelerated in the first half of the 2000s [e.g., *Stearns and Hamilton*, 2007; *Howat et al.*, 2008; *Christoffersen et al.*, 2012]. A difference between KF and SF is that there is no channel running across the mouth of KF as at SF; instead a deep sill (∼450 m) obstructs the connection from the trough into the fjord (Figures 1 and 2).

SF and KF lie in the southeastern sector of Greenland that abuts the Irminger Sea, which receives relatively warm and salty subtropical-origin water via the Irminger Current, as well as colder and fresher polar-origin
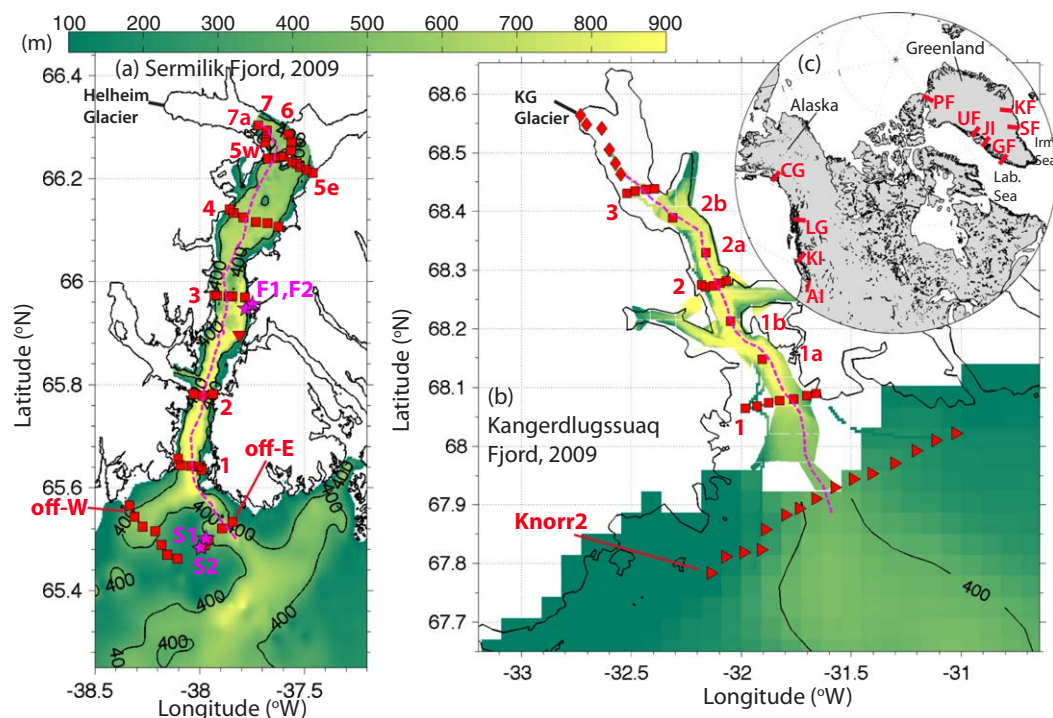
Figure 1. (a) Map of Sermilik Fjord (SF) coastline and bathymetry with locations of 2009 CTD/LADCP profiles (red squares) and the 2009–2010 moorings on the shelf: S-1 and S-2, and in the fjord: F-1 and F-2 (magenta stars). Bathymetry is a combination of *Schjøth et al.* [2012], IBCAO v.3, and seal-derived data [*Sutherland et al.*, 2013]. Note some shallow regions near the coast are based on zero data and may not be accurate. Red dashed line follows the thalweg from offshore toward the glacier front. (b) Same as in Figure 1a, but for Kangerdlussuaq Fjord (KF) 2009 data. Stations 1a, 1b, 2a, and 2b were occupied along fjord between the cross-fjord transects and XBT profiles (diamonds) were made through the ice mélange near the glacier. A 2008 section occupied by the *R/V* Knorr is shown (Knorr2: triangles). (c) Overview map showing additional glaciers discussed in Greenland including Uummannaq Fjord (UF), Godthabsfjord (GF), Petermann Fjord (PF), and Jakobshavn Isbrae (JI), as well as Columbia Glacier (CG), LeConte Glacier (LG), Knight Inlet (KI), and Admiralty Inlet (AI) outside Greenland.

water from the north via the East Greenland Current [*Rudels et al.*, 2002; *Sutherland and Pickart*, 2008]. The Irminger Current retroflects at Denmark Strait and joins the Arctic outflow; the composite flow is referred to as the East Greenland/Irminger Current (EGC/IC), which advects polar water (PW) and Atlantic-origin water (AW) equatorward along the shelf break of SE Greenland. Both the KF trough and the canyon leading to SF affect the EGC/IC, causing it to veer toward the coast [*Sutherland and Pickart*, 2008; *Magaldi et al.*, 2011], leading to an intrusion of AW far onto the shelf toward SF and KF. The EGC/IC current system is baroclini-cally unstable and an energetic mesoscale eddy field is apparent in observations [*Bruce*, 1995; *Brearley et al.*, 2012] and model simulations of the SE Greenland shelf [*Magaldi et al.*, 2011], which provides another mech-anism for transport of AW toward the coast. An inner branch of the EGC, the East Greenland Coastal Current (EGCC), is often found in immediate proximity to the Greenland coast, carrying roughly 1 Sv of water and ∼50–60 mSv of freshwater, relative to a reference salinity of $S_{ref} = 34.8$ [*Bacon et al.*, 2002; *Sutherland and Pickart*, 2008]. This current has been observed both upstream and downstream of SF, and limited observa-tions suggest it is steered through the narrow channel outside the mouth of SF [*Sutherland et al.*, 2013].

The geometries of SF and KF are not uncommon for Greenland's glacial fjords, although Helheim and Kan-gerdlugssuaq Glaciers are relatively large compared to other glacier systems (Figure 1 and Table 1). For example, the average cross-sectional aspect ratio $A_{cross} = B_m/H = 0.13$ for SF and 0.14 for KF (Table 1, where B_m is mean fjord width and H is mean fjord depth), similar to values for Jakobshavn Isbrae [*Schumann et al.*, 2012; *Holland et al.*, 2008], Godthabsfjord [*Mortensen et al.*, 2011], and two systems in the Uummannaq region of west Greenland, Sermeq Avangnardleq [*Rignot et al.*, 2010] and Rink Isbrae [*Roberts et al.*, 2013]. The sill depths are slightly deeper in SF and KF ($H_s/H_{max} > 0.5$, where H_s is sill depth and H_{max} is the maxi-mum fjord depth) than in other Greenland fjords (with the exception of TOR). Petermann Fjord is wider than SF or KF, but with a similar H_s/H_{max} value compared to the Greenland fjords listed—the major differ-ence, of course, being the large ice shelf that Petermann Glacier supports [*Johnson et al.*, 2011]. However, all
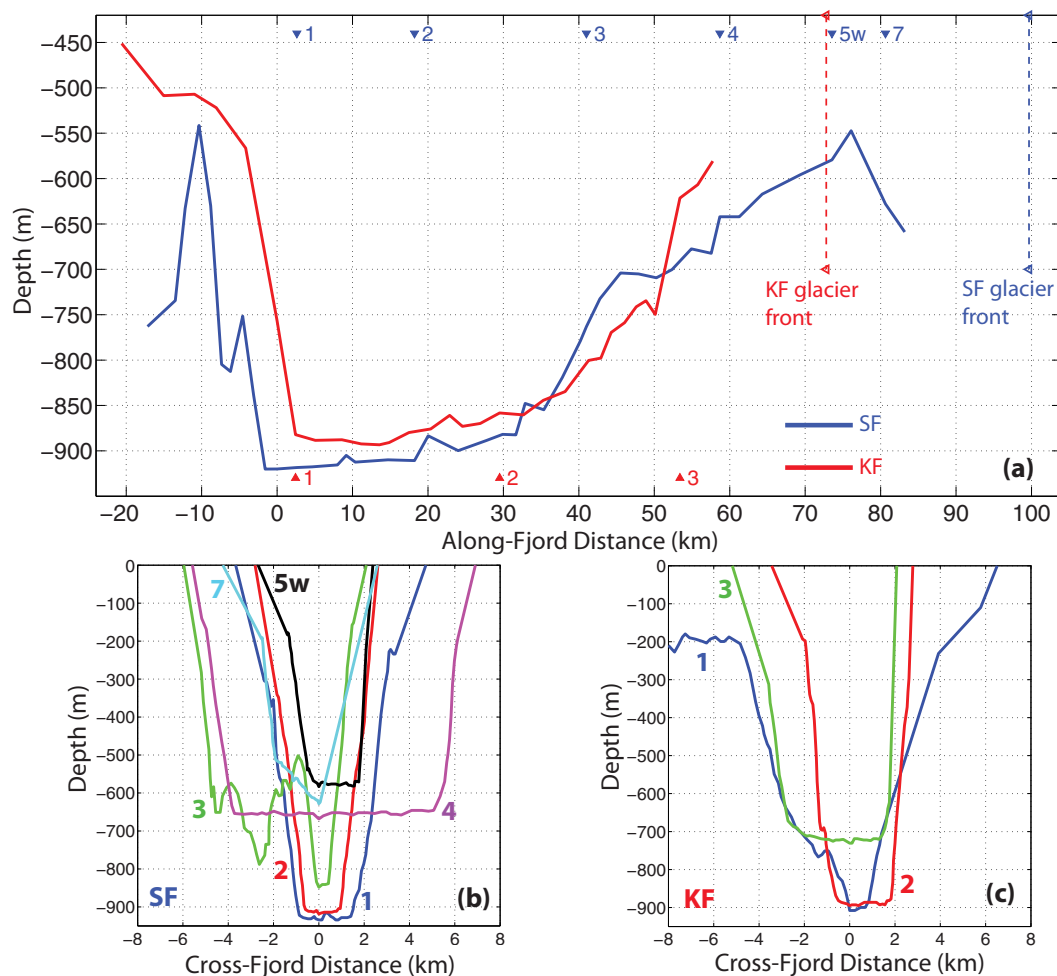
Figure 2. (a) Transects of seafloor depth taken along each fjord thalweg (maximum depth) shown by the black dashed line in Figure 1. Numbers correspond to across-fjord sections (Figure 1) from outside the mouth toward the glacier from left to right. No data are available close to the glacier front due to the presence of ice mélange. Approximate locations and depths of each glacier are indicated. (b) Bathymetric cross sections in Sermilik Fjord taken along CTD sections (Figure 1) with $x = 0$ at deepest depth. (c) Same as in Figure 2b for KF Fjord.

the Greenland fjords listed in Table 1 have deep sills compared to tidewater glacial fjords in Alaska, such as LeConte Glacier [*Motyka et al.*, 2003] or Columbia Glacier [*Walters et al.*, 1988]. Puget Sound in Washington, USA, is similar in cross-sectional aspect ratio, but has a deeper sill in Admiralty Inlet [*Geyer and Cannon*,

Table 1. Physical Characteristics of SF and KF Compared to Other Fjord/Glacier Systems Across Greenland, Alaska, and the Pacific Northwest in the USA and Canada

Name	Location	H_s[a] (m)	L (km)	B_m[b] (km)	A_{cross}[c]	H_s/H_{max}[d]
Sermilik	SE Greenland	550	100	6	0.13	0.59
Kangerdlugs.	SE Greenland	450	75	6	0.14	0.52
Jakobshavn I.	W Greenland	265	60	7	0.11	0.33
Godthabsfjord	W Greenland	170	170	4	0.10	0.28
S Avg. (TOR)	NW Greenland	300	20	4	0.10	0.55
Rink Isbrae	NW Greenland	420	50	5	0.20	0.38
Petermann	N Greenland	380	80	15	0.07	0.38
LeConte	SE Alaska	20	20	1	0.25	0.07
Columbia	SE Alaska	20	20	3	0.07	0.08
Puget Sound	WA, USA	65	100	3	0.07	0.26
Knight Inlet	BC, Canada	60	75	1	0.40	0.12

[a]Depth (m) of the shallowest sill between the fjord mouth and the glacier face.
[b]Average width (km) of main fjord channel.
[c]Calculated as mean fjord depth (not sill depth) divided by mean fjord width.
[d]Ratio of sill depth to maximum fjord depth (H_{max}).

1982; *Sutherland et al.*, 2011], while Knight Inlet, BC, Canada, is exceptionally narrow and deep [*Farmer and Freeland*, 1983].

Three major factors likely contribute to making the summer circulation in Greenland fjords different from that of other typical fjords and estuaries. First, the freshwater forcing that drives the buoyancy-driven flow is different both in character and in magnitude from that of typical estuarine fjords. Notably, a large fraction of the freshwater is input in summer at the glacier's base as subglacial discharge (Q_{sg}) – often hundreds of meters below sea level. Estimates of Q_{sg} are largely uncertain, due to the challenges of observing it directly, and are typically calculated by assuming that the runoff estimated from a surface mass balance model drains to the glacier bed and enters the fjord subglacially [*Mernild et al.*, 2012]. Other liquid freshwater terms, such as the surface runoff that does not drain to the bed and iceberg melt, are assumed smaller than Q_{sg}, though direct estimates of these are also uncertain. Second, the mixing of this subglacial discharge into the fjord's waters is strongly modulated by the interaction between the upwelling buoyant plumes in front of glaciers and the ambient stratification of these deep fjords, which typically mimics the stratification on the shelf and is due to the large property differences between Arctic and Atlantic waters [*Straneo et al.*, 2012]. This means that as the subglacial discharge upwells and entrains ambient water along the glacier face, it may reach neutral density before reaching the surface [*Straneo et al.*, 2011; *Sciascia et al.*, 2013]. The neutral density depth varies with the ambient seawater stratification and the magnitude of Q_{sg}, so a time-varying estuarine circulation could affect different layers of the fjord. Third, the relatively deeper connections ($H_s/H_{max} > 0.25$) imply that exchange in the fjords might not be limited to buoyancy-driven dynamics forced by the glacier, but could include intermediary circulation that is externally forced by the coastal ocean.

2.2. Fieldwork
2.2.1. Hydrographic and Velocity Data

A summertime 2009 research cruise aboard the *M/Y Arctic Sunrise* collected the majority of the hydrographic and velocity data used in this study. The cruise ran from 19 August 2009 to 1 September 2009, occupying 42 stations in SF, 10 stations outside the mouth of SF, and 21 stations in KF (Figure 1). At each station, conductivity/temperature/depth (CTD) profiles were obtained with a 6 Hz XR-620 RBR sensor that was calibrated pre and postdeployment. The hydrographic data for SF have been described previously [*Straneo et al.*, 2011]. During each CTD profile, velocity data were simultaneously collected using a 300 kHz RDI lowered acoustic Doppler current profiler (LADCP) system. The velocity data were binned into 20 m depth bins after removing the ship motion and corrected for local magnetic declination. A subset of these LADCP data were reported earlier in SF, but not for KF [*Sutherland and Straneo*, 2012].

Since no offshore sections were occupied in 2009 outside KF, we rely on a previous research cruise for data there. In October 2008, the R/V Knorr (cruise 194, Leg IV) collected CTD and hull-mounted ADCP data along a 15-station transect immediately outside the KF mouth (Figure 1) [*Pickart*, 2008]. The hydrographic data were obtained with a Seabird 911+ CTD system. Salinity bottle samples were used to calibrate the CTD conductivity sensor (accuracies are 0.002 for salinity and 0.001°C for the temperature sensor). The ship was equipped with both a 75 and 300 kHz RDI ADCP running continuously during the cruise.

All of the CTD station data, consisting of salinity (S) and temperature (T), were pressure averaged to a resolution of 2 dbar. We then constructed vertical property sections at each transect by interpolating those data onto regular grids, with varying horizontal resolution of 0.5–2 km in the horizontal (section dependent) and 5 m in the vertical, using a Laplacian-spline interpolation scheme [e.g., *Sutherland and Pickart*, 2008]. Potential density (σ_θ) and potential temperature fields, referenced to the sea surface, were constructed from the gridded sections at identical spacing. All temperatures reported hereafter are potential temperatures. Relative geostrophic velocities (U_{geo}) were calculated from the potential density fields, using a reference velocity of zero at the seabed, i.e., at the minimum depth between two neighboring vertical profiles (these were subsequently referenced using the ADCP data, see below).

2.2.2. Bathymetric Data

Obtaining accurate bathymetric data inside SF and KF is challenging. For example, the best high-resolution product for the Arctic Ocean region, the International Bathymetric Chart of the Arctic Ocean (IBCAO v3) [*Jakobsson et al.*, 2012], has linearly interpolated values from the shelf break to the coast in the vicinity of these fjords, suggesting very shallow regions instead of the deep, U-shaped fjords shown in Figure 1. We

base our bathymetry on data compiled by *Schjøth et al.* [2012] for SF and from available multibeam data for KF (available from the British Oceanographic Data Centre: http://www.bodc.ac.uk/). For the shelf regions outside the mouths of each fjord, we blend the fjord data with the IBCAO product, and include depths derived from deep-diving seals [*Sutherland et al.*, 2013]. This combination of data shows the small-scale (<5 km) channels and deep features of these fjord systems and their connections to the shelf.

2.2.3. The 2009–2010 Mooring Data

Times series of *T*, *S*, and velocity come from two moorings in SF, F1 and F2, and two moorings outside the fjord in the channel running across its mouth, S1 and S2 (Figure 1). The moorings were deployed in August 2009 and recovered in August 2010. At the shelf sites, the moorings were identical and consisted of a Nortek deep water Aquadopp current meter that recorded velocity in hourly intervals, and a Seabird Micro-CAT(+P) SBE37-SM instrument that measured *S*, *T*, and pressure in 15 min increments. At S-1, the current meter was at a mean depth of 301 m and the MicroCAT at 294 m (see Figure 5). At S-2, the current meter was at a mean depth of 243 m and the MicroCAT at 224 m. At all mooring sites the current meters were placed ∼4–5 m above the bottom in an attempt to keep them low profile and avoid ice damage.

Inside the fjord, there was a shallow mooring (F-1) that consisted of a Nortek deep water Aquadopp current meter at 141 m, and a Seabird MicroCAT(+P) SBE37-SM instrument that measured *S*, *T*, and pressure in 15 min increments at a mean depth of 119 m. A second mooring recorded data at depth (F-2), with the current meter at 622 m and the MicroCAT at 608 m. The moored *T* and *S* data were calibrated with CTD casts taken during the deployment and recovery cruises.

2.2.4. Meteorological Data

Wind data come from the global NCEP Reanalysis product provided by the NOAA/OAR/ESRL PSD, Boulder, Colorado, USA (http://www.esrl.noaa.gov/psd/) [*Kalnay et al.*, 1996] for a region outside each fjord mouth. For SF, positive along-shelf winds are directed along 216°T. Calculated wind stresses, τ (N m^{-2}), come from the *Large and Pond* [1981] formulation (northeasterly downwelling-favorable winds: $\tau > 0$). Outside KF, positive along-shelf winds are directed along 250°T. Along-fjord winds are taken to be in the same direction that the main fjord channel runs (16°T for SF, 340°T for KF). In the along-shelf direction, the strongest winds, typically exceeding 15 m s^{-1}, occur during barrier wind events that develop when air is blocked by the Greenland continent and strong winds flow toward the southeast [*Harden et al.*, 2011].

During the time period of this study, along-fjord winds were small (as observed from the ship), although two barrier wind events occurred near the time of the cruise. One event preceded the SF survey, peaking early on 19 August 2009 with wind stress magnitudes of 0.1–0.3 N m^{-2}. The survey started that same day near midfjord in SF, proceeded up fjord toward the glacier, then headed back toward the shelf occupying the mouth section on 24 August 2013. A second stronger wind event occurred during the shelf sections and on the transit to KF, peaking at 0.4 N m^{-2} on 25 August 2009, which preceded the KF survey that took place from 28 August 2009 to 31 August 2009. On the time scales of these barrier wind events, each individual section occupied was synoptic, but the time period between sections and between fjords is on the same time scale as the wind variability.

2.3. Tidal Analysis and Velocity Data Processing

Direct observations of velocity are rare in Greenland's fjords. For each current meter, the T-Tide package in MATLAB [*Pawlowicz et al.*, 2002] was used to run a harmonic analysis on the complex velocity time series (supporting information, Table S1). The M$_2$ semidiurnal lunar constituent has the largest amplitude at each site, both inside and outside the fjord. However, the M$_2$ magnitude of ∼0.03 m s^{-1} at the shelf sites is an order of magnitude higher than inside the fjord (Table S1). The next largest constituents on the shelf are S$_2$ (∼0.01 m s^{-1}) and K$_1$ (∼0.01 m s^{-1}). In the fjord, the S$_2$ (<0.01 m s^{-1}) and MSf (<0.01 m s^{-1}) constituents characterized the shallower current meter at F-1, while K$_2$ (<0.01 m s^{-1}) and L$_2$ (<0.01 m s^{-1}) were second and third largest for the deeper current meter at F-2.

These results compare well overall (supporting information, Figure S1) to predictions made with an Arctic Ocean inverse barotropic tidal model (AOTIM) [*Padman and Erofeeva*, 2004]. We restrict the comparison to only the shelf sites where bathymetry in AOTIM is reasonably accurate. Slight discrepancies exist for K$_1$ and S$_2$, but we cannot discern if these are due to inaccurate depths used by the model over the Greenland shelf or due to baroclinicity in the observed velocities. What is clear, however, is that the tidal

velocities inside the fjord are very weak, and are much smaller than the velocities measured during the shipboard surveys.

The tidal analysis results were used to detide each LADCP cast by subtracting out a barotropic tidal current prediction from each profile. Following this, the detided LADCP profiles were used to construct sections of cross-transect velocity on the same grid as the hydrographic variables. This rotated velocity, U_{adcp}, is in the same direction as the calculated geostrophic velocity, U_{geo}. Next we interpolated U_{adcp} onto the geostrophic velocity grid (at midway points between each profile of density). Finally, we constructed an absolutely referenced velocity field, U_{abs}, by matching the depth averages of U_{adcp} and U_{geo} over the available U_{adcp} depth range. For the 2008 Knorr section, the method to produce U_{abs} is similar, but the U_{adcp} velocities are restricted to the upper 200 m.

Using the hydrographic and velocity data, we calculate the freshwater flux, Q_{FW},

$$Q_{FW} = \int\int U(x,z)\frac{(S_{ref}-S(x,z))}{S_{ref}}dxdz, \tag{1}$$

where the velocity U is either U_{abs} or U_{geo}, and S_{ref} is 34.8. The heat transport, Q_θ, is calculated as

$$Q_\theta = \rho_0 C_p \int\int U(x,z) \cdot [T(x,z)-T_f]dxdz, \tag{2}$$

where the velocity field U is either U_{abs} or U_{geo}, and T_f is freezing point temperature that is function of S and pressure.

3. Results

3.1. Hydrographic and Velocity Sections
3.1.1. Along-Fjord Sections

The hydrographic characteristics have been described in general for SF [*Straneo et al.*, 2010; *Straneo et al.*, 2011] and for KF [*Andrews et al.*, 1994; *Azetsu-Scott and Tan*, 1997; *Christoffersen et al.*, 2011, 2012; *Inall et al.*, 2014]. We therefore only summarize them here. In both fjords, relatively cold and fresh PW is found at depths of ∼100–200m above a thicker layer of warm, salty water AW (Figure 3). As noted in the earlier studies, property variations mostly occur in the along-fjord direction—consistent with the fact that the fjord width is of the order of a deformation radius (typically <8 km). Atlantic waters in SF are considerably warmer than those in KF due to the nature of AW inflow. Two distinct AW types enter KF, a deeper, colder AW that has come through Denmark Strait after circulating around the Nordic Seas, and a warmer, intermediate AW (∼300–400 m) from the subpolar gyre which has crossed the southeast Greenland shelf from the Irminger Sea [*Azetsu-Scott and Tan*, 1997; *Straneo et al.*, 2012; *Christoffersen et al.*, 2012; *Inall et al.*, 2014]. In contrast, AW inflow to SF is dominated by the Irminger Sea type AW. This gives KF more of a three-layer vertical structure (discussed further below) compared to the largely two-layer SF, with both fjords having a thin, summer only surface layer (often called warm Polar Surface Water, PSWw) modified by surface melt and solar insolation [e.g., *Inall et al.*, 2014; *Christoffersen et al.*, 2012].

Aside from the absolute values, the change in properties from the mouth to the head of each fjord is similar (Figure 3) and indicative of the competition between shelf forcing and glacial forcing, respectively. This is apparent in the generalized cooling and freshening of properties toward the glacier and, in particular in the cold, fresh surface layer found at the head of both fjords (Figures 3 and 4). Temperature-salinity diagrams show this in the transition of properties from the mouth to those observed at the head of the fjord (Figure 4). Near the mouth, properties largely reflect the presence of the shelf AW and PW, while near the glacier there is a mixture of submarine melt, ambient water and subglacial discharge. The glacially modified waters are found within a triangle bounded by the "melt line" (mixing line for ambient water and submarine melt) and the runoff line (mixing between ambient water and subglacial discharge), Figures 4c and 4d [see also *Straneo et al.*, 2011]. In both fjords, glacially modified waters are observed at depth (as well as at the surface) consistent with the notion that a fraction of the relatively light glacial melt from the glacier's base will equilibrate (reach neutral stability) in a stratified fjord prior to reaching the surface [e.g., *Sciascia et al.*, 2013].
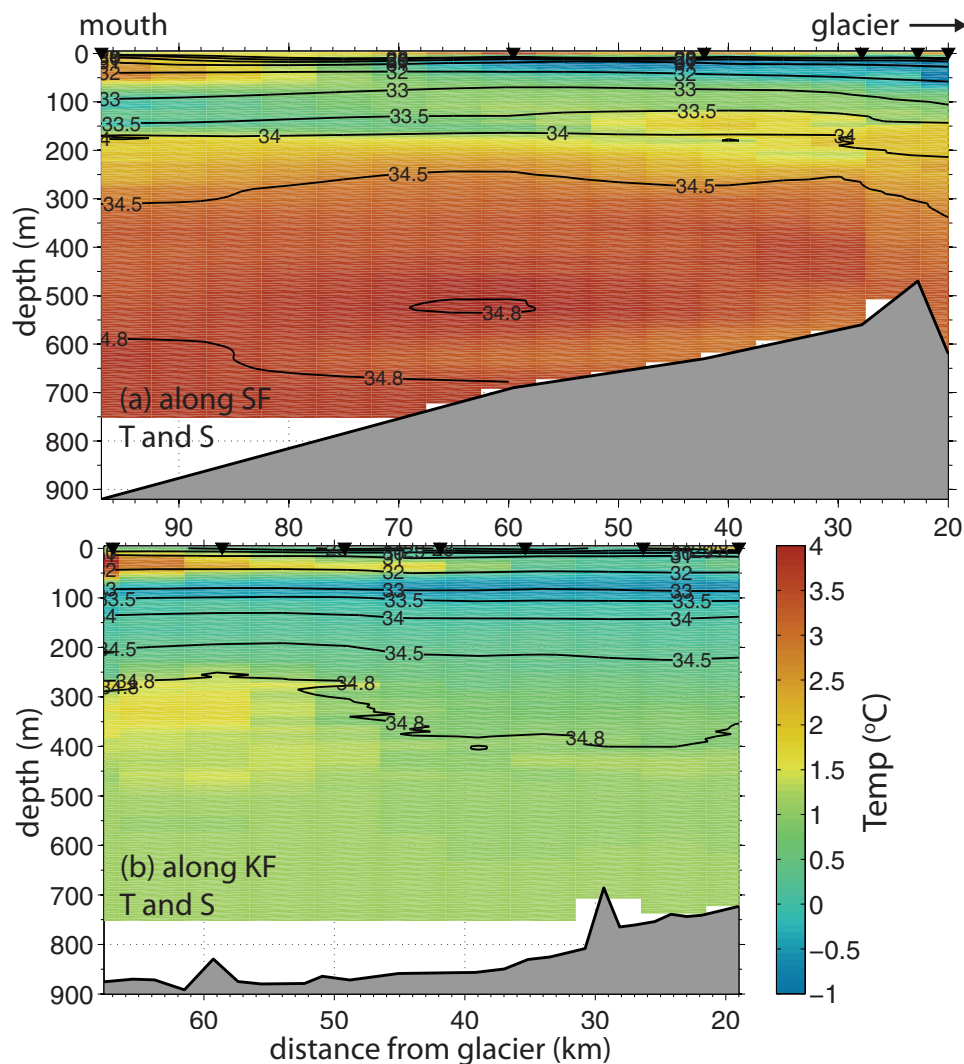
Figure 3. Along-fjord sections. (a) Potential temperature (T, °C) versus depth (color) for Sermilik Fjord with salinity, S, overlaid (black contours). Black triangles mark station locations. Distance is indicated from the glacier face. (b) Same as in Figure 3a, but for Kanglerdlugssuaq Fjord. Note the color scale and y axis are the same for both plots, but the x axis changes slightly.

3.1.2. Offshore Sections

The sections outside SF sampled a 600 m deep channel that cuts across the mouth (Figures 1 and 5). In both sections, the T and S fields show a wedge-shaped structure (Figures 5a and 5b) that is suggestive of a buoyancy-driven, equatorward coastal current and consistent with recent studies [*Bacon et al.*, 2002; *Sutherland and Pickart*, 2008]. The sloping isohalines mimic the density field and are able to support a geostrophic current comprised of relatively fresh ($S < 34$) and cool ($T < 0$°C) water, beneath a summer mixed layer with warmer temperatures (Figures 5c and 5d). This is confirmed by the absolute geostrophic velocities. At section Off-E, U_{abs} is surface intensified with peak speeds >1 m s^{-1} directed equatorward in the along-shelf sense. U_{abs} is strongest over the deepest part of the channel closer to the mouth and quite weak below 200 m depth. Just downstream at section Off-W, U_{abs} is also surface intensified with similar speeds, but the flow is strongest above the slope of the submarine bank offshore of the channel and mouth (Figure 5d). On the bank, a depth averaged flow of ~0.3 m s^{-1} is observed, implying strong barotropic flow in a region with relatively little horizontal density gradients.

Taken together, the hydrography and velocity fields observed outside SF's mouth indicate that the EGCC, interpreted as an inner branch of the EGC [*Bacon et al.*, 2002; *Jakobsen et al.*, 2003; *Sutherland*
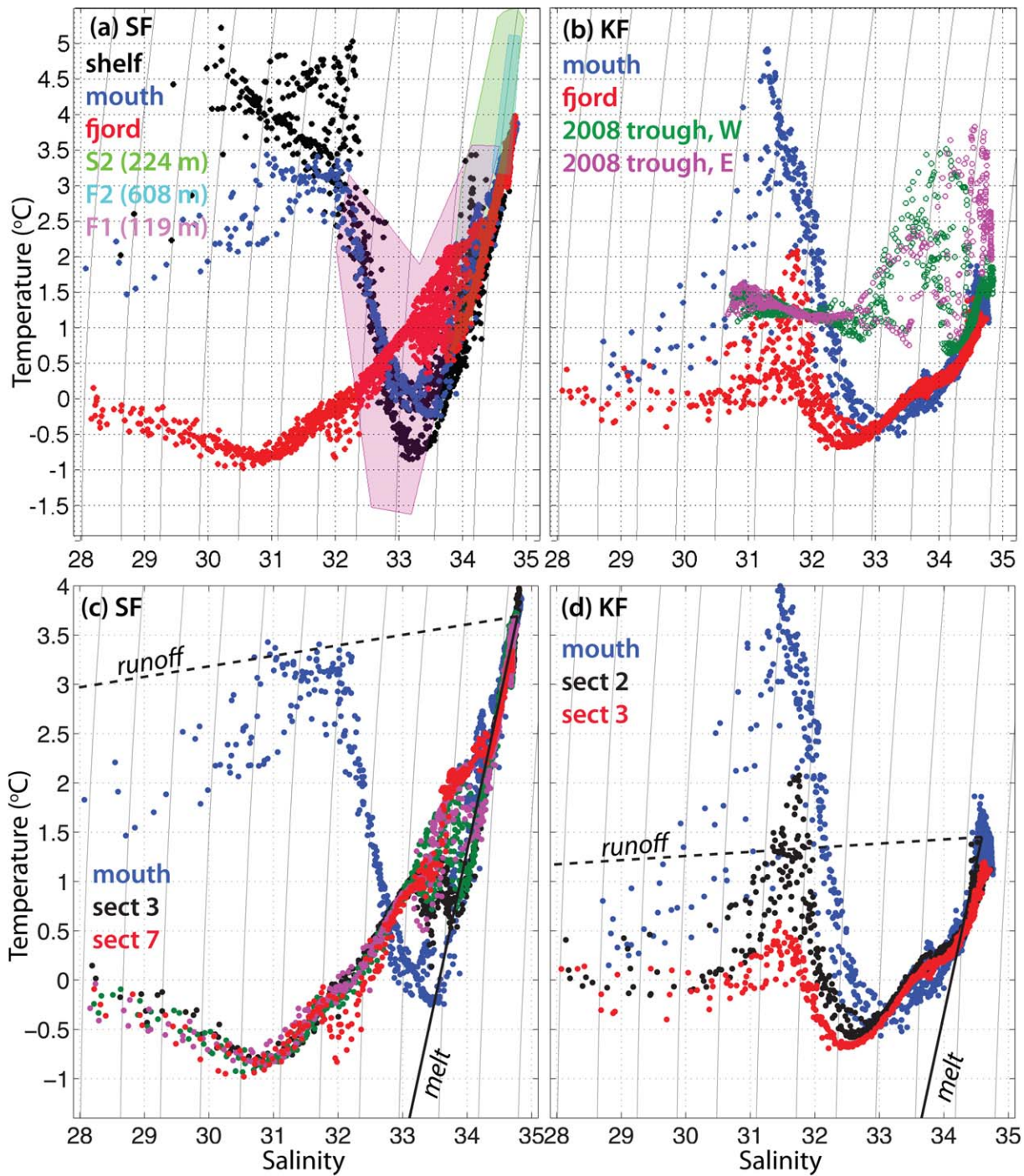
Figure 4. (a) Temperature-salinity diagram for the summer 2009 Sermilik Fjord data comparing the mouth (blue), shelf (black), and the remaining fjord sections (red). Shaded regions indicate the range of *T-S* measured at moorings inside the fjord, F-1 (magenta) and F-2 (cyan), and on the shelf, S-2 (green), over the entire year 2009–2010. (b) Same as in Figure 4a, but for Kangerdlugssuaq Fjord. Note there were no shelf sections in 2009, so a 2008 KF trough transect is shown, divided into east (magenta) and west (green). (c) Zoom-in on the SF *T-S* diagram shown in Figure 4a, focused only on the fjord sections. Runoff and meltwater mixing lines are indicated. (d) Same as in Figure 4c, but for KF.

and Pickart, 2008], flows through the narrow channel outside of SF. Thus, contrary to the interpretation of *Inall et al.* [2014], we find evidence of a deep connection to the shelf break, where a ~450 m deep sill exists, that steers the EGCC through 600 m deep channels adjacent to the mouth of SF. The total volume transports, *Q*, at sections Off-E and Off-W are 0.9 and 1.0 Sv, respectively, though this includes flow over the shallow bank (Table 2). *Sutherland and Pickart* [2008] restricted their volume budget for the EGCC to waters with $S < 34$. Doing the same for Off-E and Off-W, and limiting the spatial extent to exclude the shallow
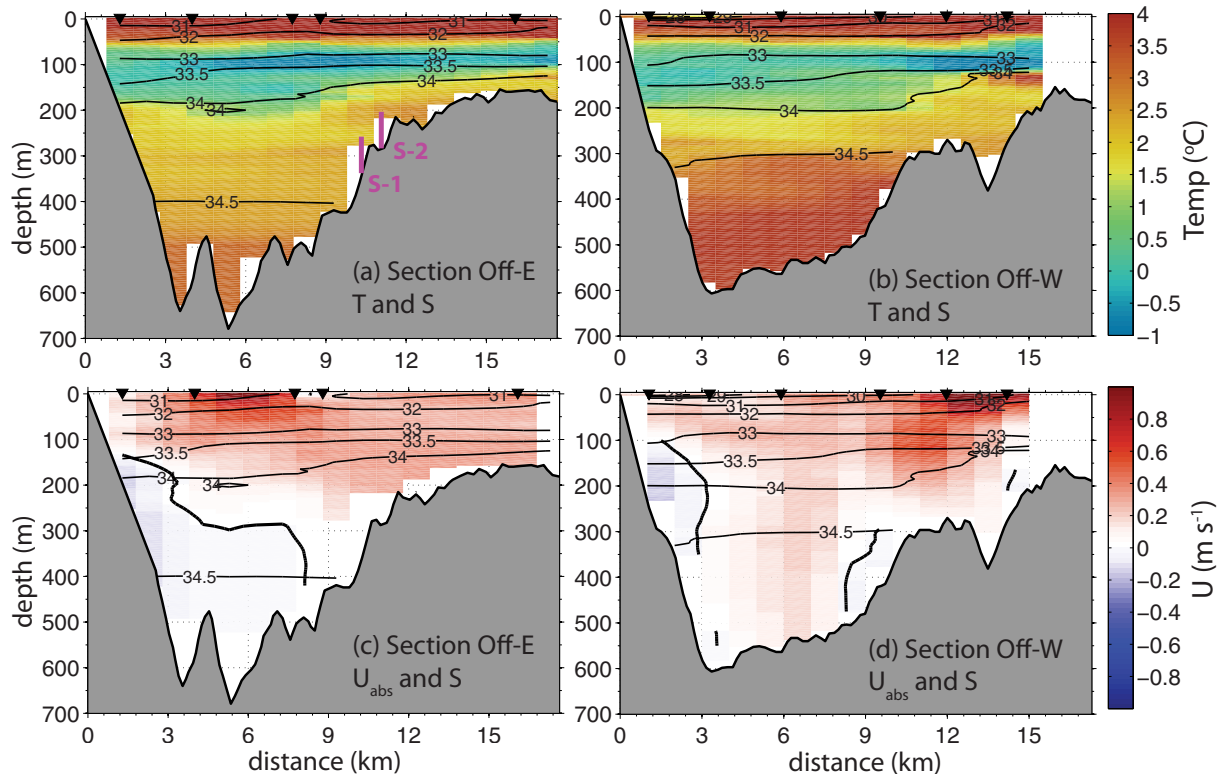
Figure 5. Offshore SF sections. (a) Potential temperature versus depth (color) for Off-E with salinity overlaid (black contours). Black triangles mark station locations. Magenta lines show approximate locations of the shelf moorings S-1 and S-2. The coast is to the left where depth goes to zero. (b) Same as in Figure 5a, but for Off-W section. (c) Absolute velocity (U_{abs}, color) versus depth for Off-E with salinity overlaid (black contours). $U_{abs} > 0$ is flow to the NW. (d) Same as in Figure 5c, but for Off-W. $U_{abs} > 0$ is flow to the SW.

bank, results in $Q^* = 0.52$ and 0.68 Sv for Off-E and Off-W, respectively, where the star indicates a transport over the limited region. These volume transports are similar to those found for the EGCC previously [*Bacon et al.*, 2002; *Sutherland and Pickart*, 2008], supporting the conclusion that the EGCC is a persistent feature with a large volume flux. The freshwater transport, Q^*_{FW}, carried by the EGCC here is 34–46 mSv.

While the flow outside SF is a mostly geostrophic coastal current directed across the mouth of the fjord, a different situation exists outside KF. The KF trough extends from the shelf break to the mouth of KF in an approximate straight line, with the deepest connection running straight into the fjord, not across it as at SF (Figures 1 and 2). Figure 6 shows a section taken across the KF trough in 2008, immediately outside the fjord mouth. The strongest signal observed in the T and S fields are inside the trough ($z > 180$ m). Here the 34.5 isohaline slopes strongly downward toward the southwest, dipping ~150 m in 20 km. Banked against the right side of the trough is the warmest water found in the section, with $T \sim 4°C$. At the same depth level on the left side of the trough one finds the coldest waters, $T \sim 0°C$, which are also fresher. Analysis of the T/S properties confirms that waters on the eastern (right) side of the trough are largely unmodified Irminger Water (Figure 4b), while waters on the western side of the trough are a mixture of Irminger Water with glacially modified water.

The lateral density gradient associated with the dipping isohalines inside the trough creates a strong baroclinic, geostrophic flow (Figure 6b). Above 180 m, the circulation is anticyclonic with peak speeds near 0.4 m s^{-1}. Inside the trough, the flow is toward the fjord on the right side of the channel (eastern side), advecting warm, salty Irminger Water shoreward. On the western side, the absolute velocity section shows a weaker flow away from the fjord, again largely supportive of the notion that a mixture of glacially modified water and Irminger Water are flowing out of the fjord on the western side of the trough. This two-way circulation inside the trough is to be expected given that the trough is much wider (~20 km) than the Rossby deformation radius (~9 km) estimated from CTD data. It also highlights the uncertainty of extending

Table 2. Volume (Q), Freshwater (Q_{FW}), and Heat (Q_Θ) Transports for SF and KF in 2009, and in the KF Trough in 2008[a]

Section	Q (Sv)	Q_{FW} (mSv)	Q_θ (TW)	Q^* (Sv)	Q^*_{FW} (mSv)	Q^*_θ (TW)
SF Sect Off-E[b]	0.9	51	6.4	0.52	34	3.8
SF Sect Off-W[c]	1.0	53	8.8	0.68	46	5.2
SF Sect 1	−0.08	−7.4	−0.8	−0.07	−7.6	−0.62
SF Sect 3	0.09	6.1	0.4	0.08	6.1	0.11
SF Sect 4	−0.01	2.3	−0.3	0.01	2.4	−0.01
SF Sect 5w	−0.06	8.5	−1.0	0.03	9.1	0.03
SF Sect 5e	−0.02	−2.7	−0.36	0.01	−2.4	−0.07
SF Sect 6	−0.02	8.9	−0.75	0.04	9.4	0.042
SF Sect 7	0.005	−3.1	0.27	−0.02	−3.3	−0.07
KF Sect 1	0.03	11.3	1.0	0.12	12.2	1.3
KF Sect 2	0.02	0.6	0.19	−0.005	0.5	0.06
KF Sect 3	−0.04	2.4	0.003	−0.003	3.3	−0.02
Knorr2 2008[d]	−0.28	−42	−1.3	0.17	0.18	1.1

[a]First three columns are over entire section, while the last three columns (starred quantities) are limited to $S < 34$, and where noted, over part of section only. For fjord sections, $Q > 0$ is in-fjord, while offshore, $Q > 0$ is in the direction of the EGCC.
[b]Sect off-E starred values calculated for region $x > 6$ km (and $S < 34$).
[c]Sect off-W starred values calculated for $x < 14$ km (and $S < 34$).
[d]Knorr2 section starred values calculated for $S > 34$ in the trough ($x > 15$ km). $Q > 0$ is toward KF fjord.

along-fjord property sections into the trough in one continuous transect [e.g., *Azetsu-Scott and Tan*, 1997; *Christoffersen et al.*, 2012] since, depending on where the stations are taken in the trough, averages may be representative of the waters flowing toward the fjord, away from the fjord, or a mixture of the two. The total transport across the section is away from KF, $Q = -0.28$ Sv (Table 2). However, to investigate the Irminger Sea water transported toward the fjord, we limit the transport calculation to $S > 34$ and $x > 15$ km. In this case, $Q^* = 0.17$ Sv toward the fjord.

3.1.3. Mouth Sections
Compared to the offshore sections, the sections taken at the mouths of SF and KF exhibit a more complex flow structure (Figure 7). At SF, the water properties are similar to those observed offshore. The distinctive features are the downward sloping 34 and 34.5 isohalines toward the west (Figure 7a) and a slight doming of the 33 isohaline. Anticyclonically recirculating water is found below 200 m, where the net transport is ∼0. The overall transport at SF section 1 is out-fjord, primarily due to the flow in the upper layer (Table 2).

In contrast to SF, the freshest water at the mouth of KF, confined to $z < 80$ m, is found on the eastern side of the fjord. Here, there is a surface intensified flow into the fjord, with no observed outflow as expected from an estuarine perspective. Below ∼300 m there is a cyclonic recirculation cell, opposite to what it observed at the mouth of SF. The depth-averaged velocities are small over the entire section (<0.1 m s^{-1}), except in the surface inflow where speeds reach 0.2 m s^{-1}. This inflow accounts for the overall in-fjord volume and freshwater transport found here (Table 2).

3.1.4. Mid-Fjord Sections
The mid-fjord section 3 in SF (Figures 8a and 8c) was occupied almost 4 days prior to the mouth section and the water masses present reflect variability that must have occurred during that time (Figure 4). The warmest and saltiest water is still in the deep layer below $z > 200$ m, but the relatively warm and fresh surface layer is much cooler ($T \sim 0°$C at section 3 versus $T \sim 1.5°$C at the mouth). The most striking difference observed mid-fjord is the velocity structure (Figure 8c), which is surface intensified, reaching 0.3 m s^{-1} into the fjord above 100 m. The flow goes to near zero in a mid-depth layer and is small, but positive, below the 34.5 isohaline ($z > 300$ m). The net transport of 0.09 Sv is directed into the fjord (Table 2), and restricting these calculations to $S < 34$ only decreases the magnitude to 0.08 Sv.

The mid-fjord section at KF (Figures 8b and 8d) shows similarities to the KF mouth section in both flow and water mass structure. The warm, subsurface temperature maximum is eroded by $>2°$C by mid-fjord (Figures 4 and 8b), and the 34.5 isohaline is deepened by almost 150 m. The flow is into the fjord at the surface over the upper 100 m on the eastern side (Figure 8d), much like at the fjord mouth. Below this layer, the flow is out-fjord between 100 and 200 m depth. There is a hint of the recirculation observed at the mouth, though
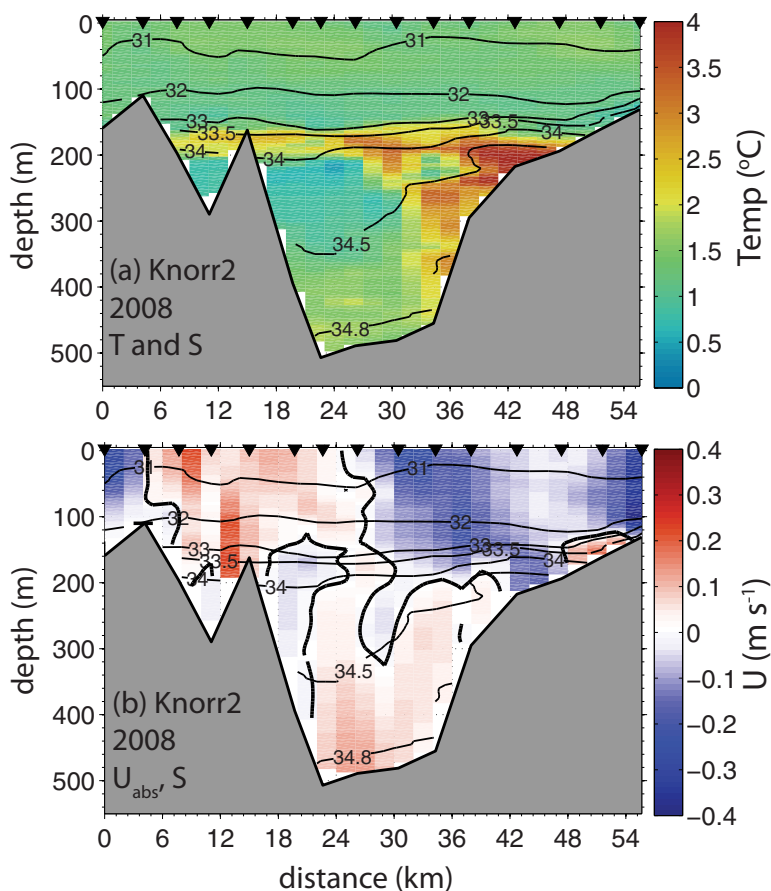
Figure 6. The 2008 Knorr2 trough section. (a) Potential temperature versus depth (color) with salinity overlaid (black contours), looking toward KF Fjord. Black triangles mark station locations. Note the change in colorbar and x scale from other section plots. (b) Absolute velocity (U_{abs}) versus depth (color) with salinity overlaid (black contours). $U_{abs} > 0$ is flow toward the fjord.

this reverses itself with depth. Small volume and freshwater fluxes are directed into the fjord, though the $S < 34$ limited transports differ significantly from the mouth section (Table 2).

3.1.5. Upper Fjord Sections

Both upper-fjord sections (Figure 9), each taken as close to the glacier front as possible, are located after significant bends in the fjord geometry. Section 7 in SF is oriented almost north-south across the mouth of Helheim Fjord (here $U < 0$ is still defined as out-fjord, oriented to the ESE), while in KF, section 3 occurs after a westward bend in the fjord, but is oriented similarly to the other KF sections (Figure 1). The water properties found at these upper fjord sections, however, do not deviate significantly from what is found mid-fjord.

One major difference is that in SF, the velocity at section 7 (Figure 9c) is primarily two-layer with a surface recirculation in the upper 100 m, in contrast to the unidirectional, albeit strongly sheared, flow at mid-fjord (Figure 8c). U_{abs} is in-fjord over the southern 1.5 km of the upper layer ($z < 150$ m) and out-fjord on the northern part. Below this recirculation, the flow is into the fjord across the transect. The overall transport is near zero, yet $Q^* = -0.02$ out-fjord with an out-fjord freshwater flux of 3 mSv (Table 2) concentrated in the fresher upper layer. In KF, the flow field U_{abs} at the up-fjord section is more complicated with a significant across-fjord gradient and vertical shear (Figure 9d). Above the 34.5 isohaline (roughly $z < 400$ m), U_{abs} is out-fjord over the middle of the fjord, but toward the glacier on each side, with similar speeds that approach 0.4 m s^{-1}. Below 400 m, a strong anticyclonic recirculation occupies the entire deep layer. The net transport over the entire section is out-fjord, with a small freshwater flux directed shoreward (Table 2).

At KF section 3, the warm layer is further eroded away (Figures 4 and 9b) and there is a large doming found in the deeper waters, illustrated by the 34.5 isohaline. At SF section 7, there is a larger volume of cooler water found in the upper 100 m, but overall the water masses are very similar to what is found mid-fjord.
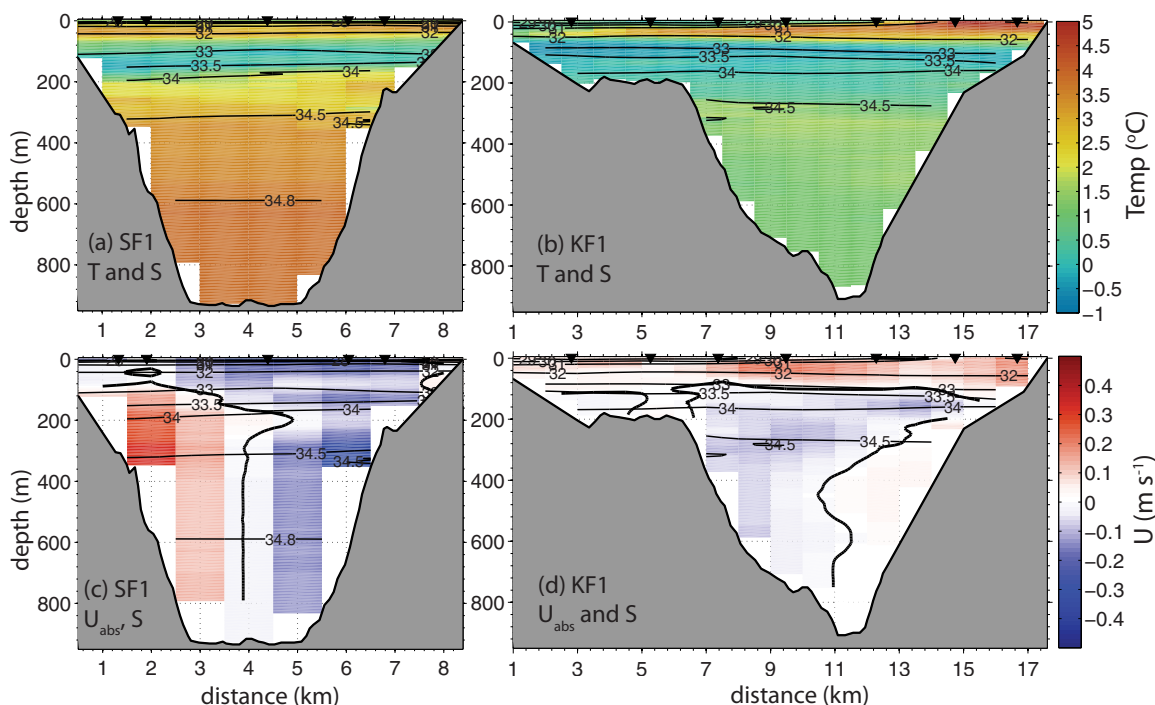
Figure 7. Fjord mouth sections. (a) Potential temperature versus depth (color) for SF-1 with salinity overlaid (black contours), looking into the fjord. Black triangles mark station locations. (b) Same as in Figure 7a, but for KF-1. Note the x scale is different for KF-1. (c) Absolute velocity (U_{abs}) versus depth (color) for SF-1 with salinity overlaid (black contours). $U_{abs} > 0$ is flow into the fjord. (d) Same as in Figure 7c, but for KF-1.
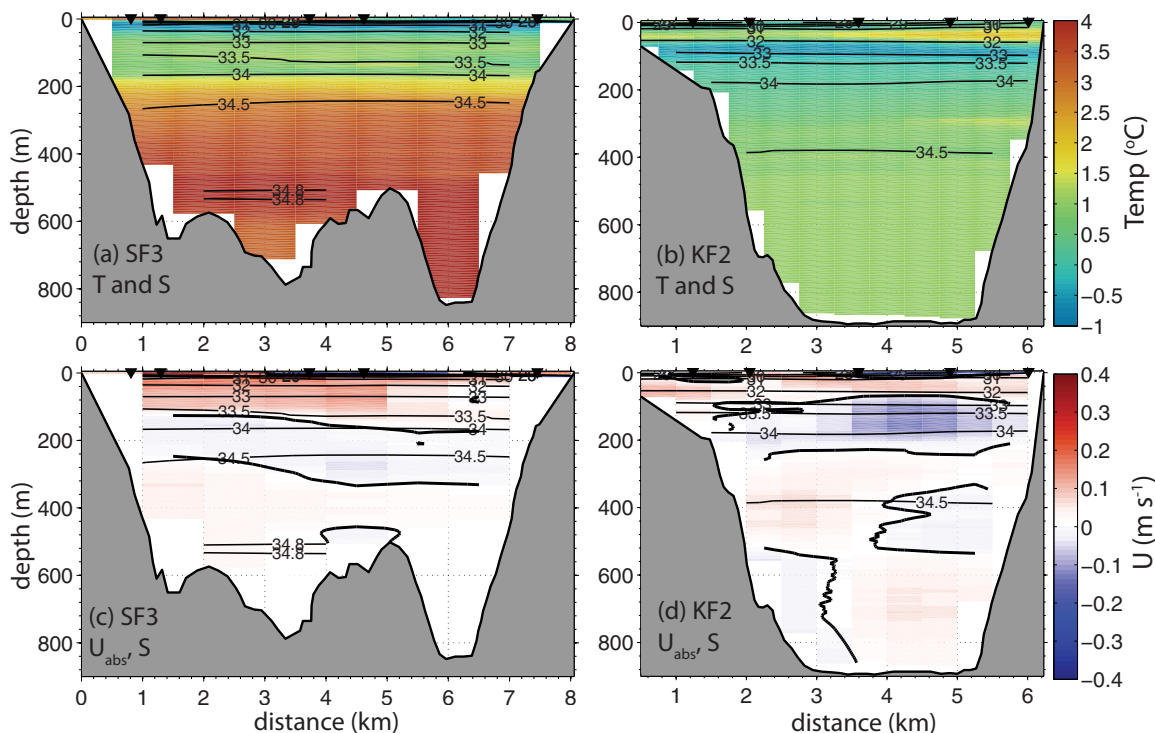

Figure 8. Mid-fjord sections. (a) Potential temperature versus depth (color) for SF-3 with salinity overlaid (black contours), looking into the fjord. Black triangles mark station locations. (b) Same as in Figure 8a, but for KF-2. Note the x scale is different for KF-2. (c) Absolute velocity (U_{abs}) versus depth (color) for SF-3 with salinity overlaid (black contours). $U_{abs} > 0$ is flow into the fjord. (d) Same as in Figure 8c, but for KF-2.
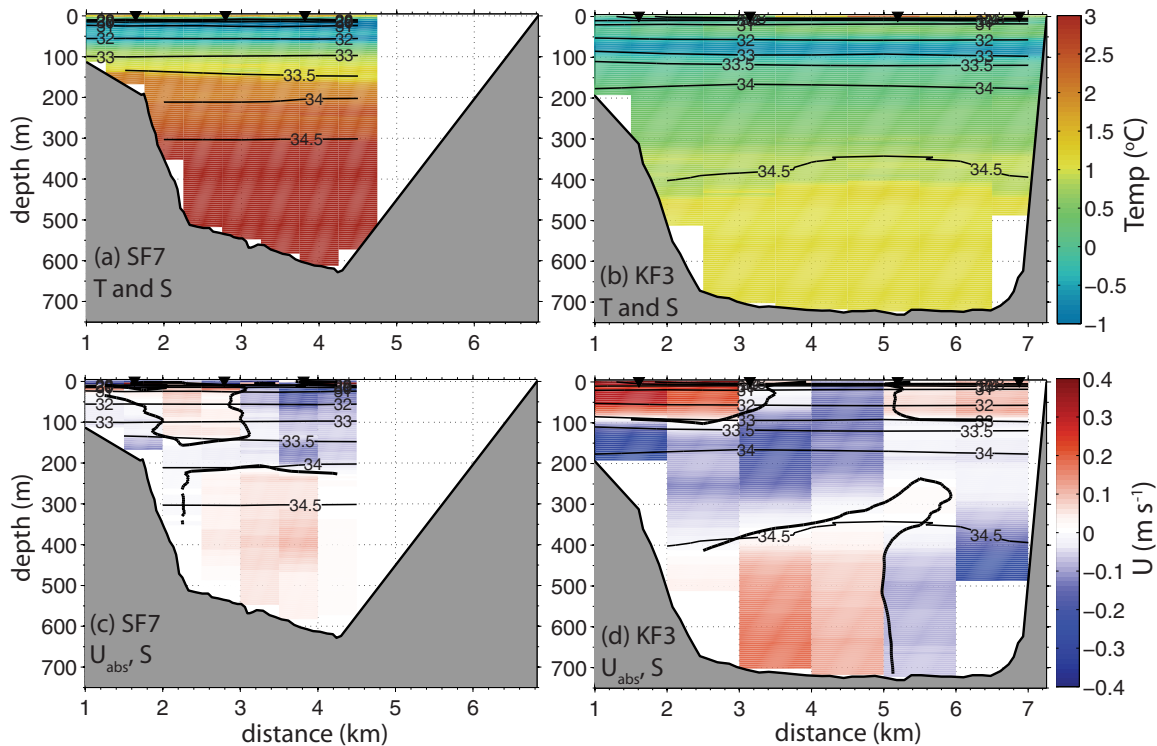
Figure 9. Upper-fjord sections. (a) Potential temperature versus depth (color) for SF-7 with salinity overlaid (black contours), looking into the fjord. Black triangles mark station locations. (b) Same as in Figure 9a, but for KF-3. Note the x scale is different for KF-3. (c) Absolute velocity (U_{abs}) versus depth (color) for SF-7 with salinity overlaid (black contours). $U_{abs} > 0$ is flow into the fjord. (d) Same as in Figure 9c, but for KF-3.

Additional sections taken in SF (sections 4, 5E, 5W, and 6; see supporting information Figures S2–S5) support the overall picture that emerges from the cross-fjord transects—a highly spatially variable flow structure with significant vertical gradients in along-fjord velocity. Time variability is aliased into the spatial variability since it took roughly 5 days to complete the survey in SF and 3 days in KF. Systematic trends in along-fjord volume and freshwater flux are not apparent (Table 2).

However, a map of freshwater content integrated from 0 to 300 m displays characteristics more in line with what one might expect in an estuarine/fjord setting (Figure 10). In SF, freshwater content decreases from the upper fjord toward the mouth. At sections 3 and 1, relatively higher freshwater content is observed on the western side of the fjord, suggestive of a geostrophically balanced plume constrained by rotational effects. The relatively high freshwater contents banked against the coast of Greenland in the offshore sections are the signature of the EGCC, with its fresher and colder waters adjacent to the coast and the underlying isohalines deepening toward the coast. At KF, the along-fjord trend of decreasing freshwater content is the same as in SF, although the overall freshwater content magnitudes are relatively smaller. At the mouth however, the high freshwater content is on the eastern edge, in line with the fresh, but warm, plume entering the fjord there (Figure 7). This small-scale plume might come from upstream as an outflow from other smaller fjords, such as Mikki Fjord or Nansen Fjord just north of KF mouth [e.g., *Jennings et al.*, 2002]. We note that the along-fjord trend of a decreasing freshwater content is robust—if the calculation is extended to 600 m depth (not shown), the trend remains the same, i.e., freshwater is not moving toward deeper depths, but seaward.

3.2. Background Circulation in Kangerdlugssuaq Fjord

The spatial variability (or aliased temporal variability) observed in the cross-fjord transects make it difficult to estimate a meaningful mean heat transport toward the glacier front, or a mean freshwater transport out of the fjord. Yet, as was done in *Sutherland and Straneo* [2012] for SF, the available LADCP profiles can be combined to create a best fit for the time-dependent flow, which can then be removed in an attempt to estimate the background circulation. What was found previously in SF is that the major mode of time-
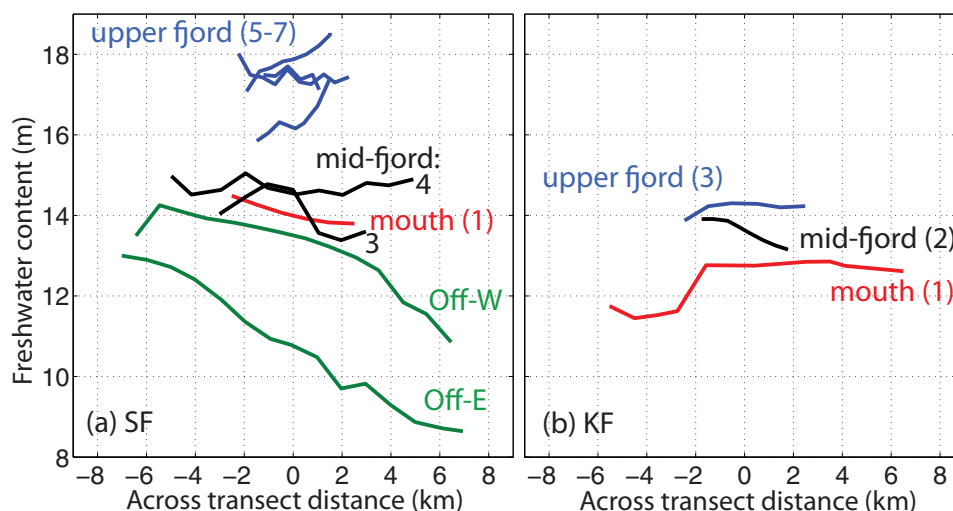
Figure 10. (a) Freshwater content (m) relative to $S = 34.8$ and integrated over 0–300 m for the Sermilik Fjord summer 2009 transects (labeled by region and number). Distance is zeroed on the center of each section looking into the fjord (eastern side on right). (b) Same as in Figure 10a, but for Kangerdlugssuaq Fjord.

dependent flow fit the intermediary circulation regime [*Straneo et al.*, 2010; *Sutherland and Straneo*, 2012; *Jackson et al.*, 2014], where wind-driven changes in the density structure on the shelf force a vertically sheared, rapidly fluctuating oscillatory flow in and out of a stratified fjord [e.g., *Klinck et al.*, 1981; *Stigebrandt*, 2012]. In summer, the intermediary circulation in SF (characterized by the first EOF of the measured velocities) corresponded to a two-layer flow. This, in turn, projects onto the first baroclinic mode as obtained from the observed density structure. In other words, SF can be characterized by a largely two-layer system. Here, we use the same method to construct a background velocity profile for KF and investigate the structure of the estuarine exchange flow pattern that emerges.

In KF, we use the 12 LADCP profiles from the mid- and upper-fjord sections (sections 2 and 3 in Figure 1), and individual casts in between these sections (labeled 1a, 1b, 2a, and 2b in Figure 1), discarding profiles from the mouth and in shallow regions where $H < 400$ m (near sides of fjord). Next, we perform a depth coordinate transformation based on each profile's stratification, as calculated from T and S profiles (Figures 11a and 11b). The transformed depth coordinate, z', goes from 0 to 1, where $z' = 0$ corresponds to the surface, $z' = 1$ to the bottom, and $z' = 0.5$ is the maximum subsurface stratification, which lies at the pycnocline (Figure 12). The end result is a series of velocity profiles on the same depth grid. An EOF analysis on this set of profiles shows the principal modes of variance present in the data. Mode 1 explains 54% of the total variance (Figure 12e), with 19% for mode 2 and 13% for mode 3. We also calculate the vertical normal mode structure based on the observed stratification profiles in z' space [*Sutherland and Straneo*, 2012].

The horizontal velocity structure of the first normal mode has a zero crossing near the interface depth at $z' = 0.5$, corresponding to the depth of maximum vertical displacement (Figure 12e). This vertical mode implies a two-layer flow, with slightly stronger velocities in the upper layer, which is thinner than the deep layer in real depth coordinates. However, the first EOF mode is not a two-layer, mode 1 flow, but has two zero crossings, one near $z' = 0.25$ and one near $z' = 0.6$. This implies a more complicated flow structure in KF than SF. In SF, the first EOF mode and first normal mode had similar shapes [*Sutherland and Straneo*, 2012]. Instead, in KF the first EOF mode more closely resembles the 2nd baroclinic normal mode, suggesting a three-layer intermediary circulation. This is consistent with the more complicated water mass layering that is present in KF, with multiple sources of AW entering the fjord. And our results are not inconsistent with the observed flow toward the glacier in the upper 50 m in KF [*Inall et al.*, 2014], suggesting that those measurements were taken at a time when either shelf winds, or other drivers of shelf variability, created an inflow in the upper layer. Indeed, this would explain why the flow at the surface is toward the glacier instead of away from the glacier, as expected from estuarine-type considerations.

To construct a background circulation profile (which is taken to be the estuarine exchange flow later in the paper), we remove a fit of the first EOF mode to each velocity profile, and then take an average over the
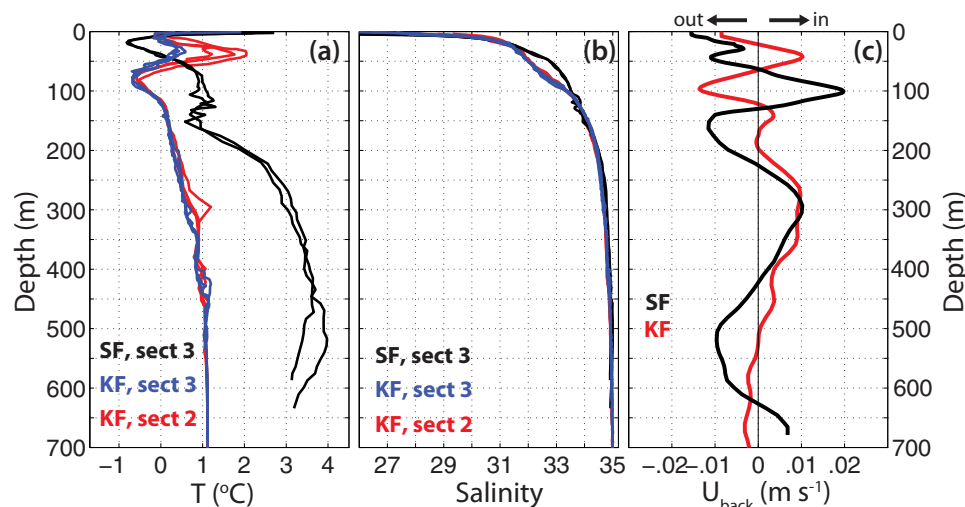
Figure 11. (a) Several typical temperature versus depth profiles from Sermilik Fjord (black) and Kangerdlugssuaq Fjord (blue, red) in summer 2009. (b) Same as in Figure 11a but for salinity. (c) Background circulation profile, U_{back}, transformed into depth space for Kangerdlugssuaq Fjord section 2 (red) compared to U_{back} from Sermilik Fjord section 3 (black) taken from *Sutherland and Straneo* [2012], with arrows indicating in or out-fjord flow.

resulting background velocity profiles. The final, adjusted velocity profile, U_{back} (Figure 11c), is extrapolated to the surface by extending the observed shear and to the bottom with a constant bottom boundary layer.

U_{back} has a peak out-fjord flow above ~20 m, with in-fjord flow between 20 and 70 m, out-fjord flow from 80 to 120 m, and a broad inflow from 200 to 500 m (Figure 11c). Here we used a mid-fjord, mid-transect profile from section 2 in KF to transform back to the true depth coordinate. The same general layering was observed in SF (Figure 11c) [from *Sutherland and Straneo*, 2012], but there are differences in the zero crossings. Another important difference is the decrease in phase speed implied by the baroclinic mode 2 structure in KF versus the mode 1 structure in SF. In the latter, the calculated phase speed, $c = 1.1$ m s^{-1}, while in KF $c = 0.6$ m s^{-1}. A slower c implies a different response to similar forcing at a certain frequency; for example, in SF, the resonant time scale based on a quarter wave oscillator for $L = 70$ km was ~71 h (~3 days). In KF, using a length of 70 km, the resonant time scale is 116 h (~5 days). Thus, the precise time scale of the external forcing generating the intermediary circulation is important, as it can excite resonant modes inside each fjord, reminiscent of internal seiches observed in other fjord systems [e.g., *Arneborg and Liljebladh*, 2001]. Both 3 and 5 days (SF and KF, respectively) lie within the synoptic weather band, so we expect both fjords to respond strongly to atmospheric forcing on the shelf. Whether other mechanisms, such as mesoscale eddies or coastally trapped waves have a preferred frequency is not known.

We do not attempt to calculate a heat transport from this background circulation profile. If we did this, and especially if we used this number to estimate a submarine melt rate for the glacier, we would effectively be assuming that the variable circulation we "filtered out" does not transport heat to the glacier. Instead, as shown by these observations, the intermediary circulation dominates the variability in both SF and KF, and its contribution to the heat transport is unknown at present; there may be a mean heat flux due to the time-dependent intermediary circulation [*Jackson et al.*, 2014]. Furthermore, the heat transported across a given section may simply warm the fjord sector upstream of it, rather than melt the glacier ice.

4. Circulation Regimes in SF and KF

4.1. Offshore Circulation Region

Using the 2009 data along with an additional 2008 section taken across the KF trough, we can classify the dominant modes of circulation in different regions of these two fjords. Immediately outside the mouth region of each fjord, the water mass and velocity structure suggest a predominantly geostrophic regime. Comparisons between ADCP-derived velocity and geostrophic velocities from each region (offshore, mouth,
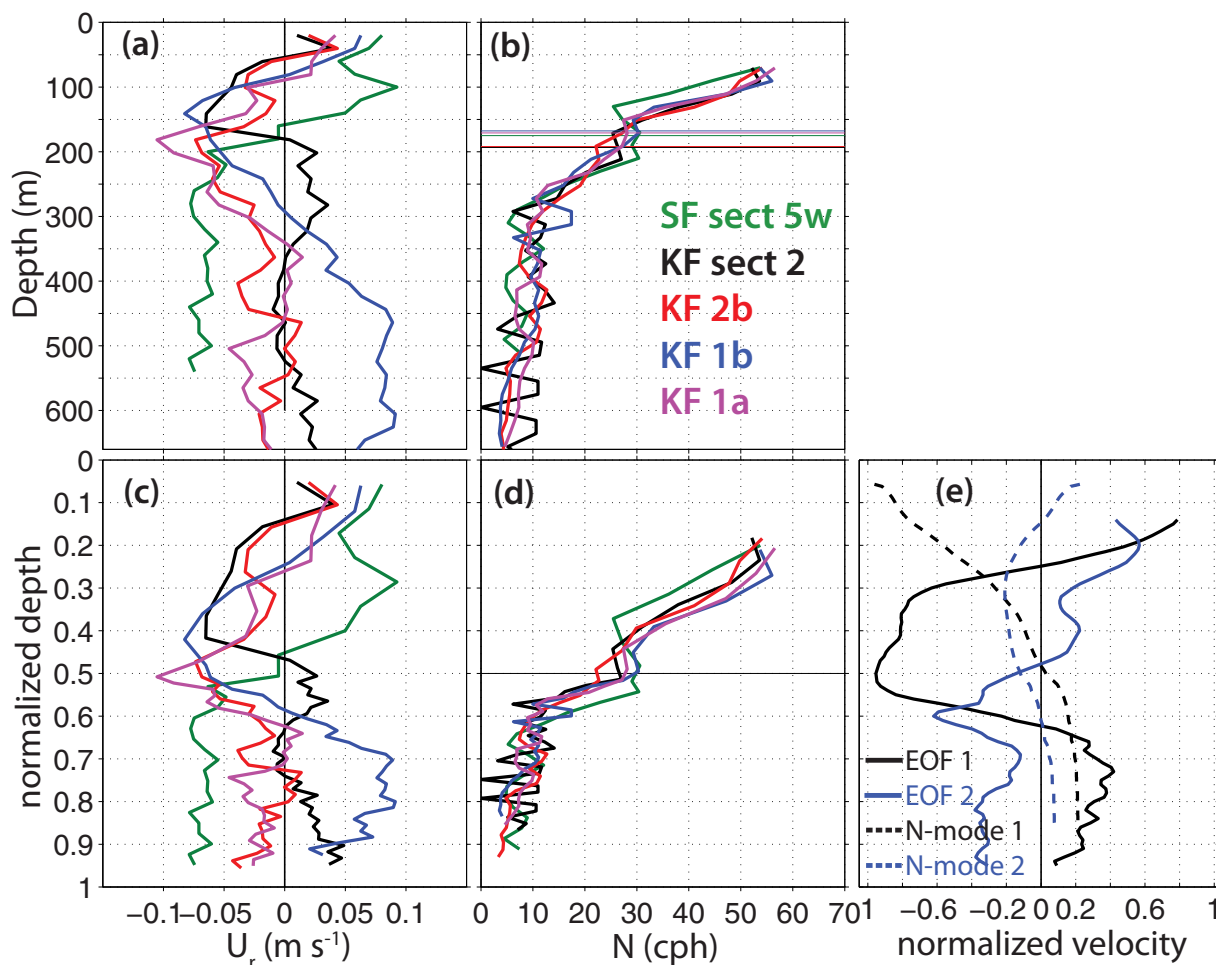
Figure 12. Examples of depth transformation at representative stations located in Kangerdlugssuaq Fjord (color) and one example from Sermilik Fjord (green) [*Sutherland and Straneo*, 2012]. (a) U_r (m s^{-1}) and (b) N (cph) in original depth space, showing the depth of maximum subsurface stratification (thin line). (c) U_r (m s^{-1}) and (d) N (cph) in z' space, the normalized depth, where the maximum subsurface stratification is at $z' = 0.5$. (e) EOF modes 1 and 2 (solid) in z' space, along with the first and second normal mode structures (dashed), normalized by the largest absolute amplitude.

mid-fjord, and upper-fjord) support this conclusion (supporting information, Figures S6–S10). Geostrophic velocity calculations match the ADCP-derived velocities better at the offshore sections and would not in general be a good estimate of velocity inside the fjords. One difference between the two systems is the way these large-scale flows impinge on each fjord. For SF, the large-scale flow is the EGCC that bends inward at the latitude of SF. The EGCC appears to flow directly across the mouth of SF. This is important to the fjord dynamics as the EGCC is sensitive to along-shelf wind forcing [*Sutherland and Pickart*, 2008], which alters the interface depth between its cold, fresh core and the Irminger Sea waters that are found beneath it. In contrast, the trough leading up to the mouth of KF runs directly into the fjord mouth, inhibiting the flow across the mouth to shallower, surface-trapped currents. A mean, geostrophically balanced current seems to exist at depth inside the trough bringing Irminger Sea water toward KF (Figure S7). However, the variability of this flow may be forced by entirely different mechanisms than those that introduce variability in the EGCC. Model results suggest that baroclinic instabilities of the EGC/IC system at the shelf break develop into anticyclonic eddies that advect onto the shelf [*Magaldi et al.*, 2011]. The time scale of this instability process is similar to synoptic wind time scales (around 3–5 days), implying that it might be difficult to untangle the two processes' impact on fjord dynamics.

Freshwater, heat, and volume budgets for the SF mouth region, based on the two offshore sections and the mouth section, balance to within 10% residuals if we restrict the calculation to the EGCC limits ($S < 34$). A volume flux of $Q^* = 0.52$ Sv flows in at Off-E while $Q^* = 0.68$ Sv flows out at Off-W (Figure 1); this is partially

balanced by an outflow from SF of $Q^* = 0.07$ Sv (Table 2). The freshwater budget is similarly balanced, with Q^*_{FW} =34mSv in at Off-E, Q^*_{FW} =46mSv out at Off-W, and Q^*_{FW} =8mSv outflow from the mouth of SF. The sum of the heat transports results in a residual of −0.6 TW, almost an order of magnitude less than the transport terms.

The magnitude of the outflows from SF, roughly 0.1 Sv of volume transport and 8 mSv of freshwater, are significantly larger than any estimate of freshwater discharge entering the fjord subglacially or via surface runoff. Freshwater discharge into SF has a magnitude of at most 1 mSv [e.g., *Andersen et al.*, 2010], with subglacial discharge (Q_{sg}) estimates closer to a quarter of that value. This observed amplification of the outflow from SF is typical of estuaries and is due to the entrainment of fluid. In Puget Sound, for example, the outflow is observed to be 20–30 times the river input into the fjord [*Sutherland et al.*, 2011]. However, in SF, it is difficult to assess this amplification factor due to the uncertainty in freshwater inputs, the impact of potential recirculations at the mouth, and the imprint of strong temporal variability on the fjord dynamics.

4.2. Intermediary Circulation Region
Inside each fjord, landward of the mouth sections, the flow is strongly sheared in the vertical (Figures 7–9) with no clear trends in volume or freshwater transport (Table 2). Taken together, we hypothesize that the mid- and upper fjord regions of both SF and KF will be dominated by the externally forced intermediary circulation [*Klinck et al.*, 1981; *Stigebrandt*, 2012]. These flows vary in time based on along-shelf wind forcing, as evidenced by time series taken in SF [*Straneo et al.*, 2010; *Jackson et al.*, 2014]. We expect them to be stronger in winter when wind forcing is greater, and any estuarine circulation subsides as Q_{sg} decreases seasonally.

Even during a single hydrographic survey, the strength of the intermediary circulation may vary. This underscores the caution with which snapshots of heat and freshwater transport must be interpreted. We see evidence for the time-varying intermediary circulation in the LADCP profiles, as profiles taken days apart show opposite vertical shear. Time series of velocity in SF support these observations, showing that fluctuating currents in the 3–6 day timeband intensify during winter in SF [*Jackson et al.*, 2014]. Time series of temperature stratification in KF suggest similar variability over the year, with heaving isotherms moving >50 m in the vertical on synoptic time scales [*Jackson et al.*, 2014]. Previous work in KF also shows that the velocity structure can have the opposite sense of flow direction compared to what is expected from a buoyancy-driven circulation [*Inall et al.*, 2014], i.e., the upper layer is flowing toward the glacier, due to the time-varying intermediary circulation.

4.3. SF and KF in Estuarine Parameter Space
Although the preceding analyses have shown that other processes may mask the estuarine circulation inside SF and KF, it is still informative to compare these fjords to other highly stratified estuaries. Characterizing SF and KF in estuarine parameter space may also allow prediction of when certain dynamics may dominate. With a long enough time series, the net circulation driven by Q_{sg} and other freshwater sources (ice melt, surface runoff, and submarine melt) should be observable.

The Wedderburn number, W, compares the energy input directly by winds to an estuary to the potential energy available for driving the baroclinic exchange flow [*Chen and Sanford*, 2009; *Geyer*, 1997]. For SF and KF fjords this is somewhat complicated by the existing stratification that changes from two-layer in SF in winter to a three-layer system in summer (counting the surface modified layer), and is four-layer in KF in summer (again, counting the thin surface layer). Nevertheless, it is instructive to calculate W as

$$W = \frac{\tau_x L}{\beta_s \Delta S g H_1^2} \ , \tag{3}$$

where τ_x is the along-fjord wind stress (N m^{-2}), L is the length of the fjord affected by the wind (length of the estuary in this case), β_s is the haline contraction coefficient, ΔS is the horizontal salinity difference averaged over the upper layer depth H_1. If $W = 1$, then the wind input and baroclinic forcing are comparable and the fjord circulation will be significantly influenced by direct wind-driven effects. Table 3 lists W for SF and KF based on two cases: using the depth of the shallow, seasonally modified glacial melt layer (GM), and using the thicker PW layer. We use a $\tau_x = 0.4$ N m^{-2}, which is the magnitude of a typical storm on the shelf.

Table 3. Estuarine Parameters for SF and KF[a]: Freshwater Forcing (Q_f), Estuarine Richardson Number Ri_e, the Freshwater Froude Number F_f, the Depth Averaged Along-Fjord Salinity Gradient, S_x, the Potential Energy Anomaly, Φ, the Wedderburn Number, W, for Two Cases, and the Critical Wind Speed to Make $W = 1$[b]

Fjord	Q_f (m^3 s^{-1})	Ri_e	F_f	$\bar{S}_x(10^{-5}$ psu m^{-1})	Φ (10^5 J m^{-2})	W GM	W PW	$U_{w,crit}$ (m s^{-1}) GM	$U_{w,crit}$ (m s^{-1}) PW
SF$_{z<Hs}$	250	400	1×10^{-5}	0.75	7.4 ± 0.9	2.0	0.2	12	27
KF$_{z<Hs}$	150	250	8×10^{-6}	0.36	9.1 ± 0.1	5.4	0.3	7	23
SF$_{all\,z}$			7×10^{-6}	0.26	6.9 ± 0.8				
KF$_{all\,z}$			5×10^{-6}	0.24	6.2 ± 0.1				

[a]For full discussion and these parameter values, see text.
[b]Average values are stated with ± 1 standard error.

For both SF and KF, we expect the wind to impact the circulation in the GM layer as $W > 1$, based on GM layer thicknesses of 20 m in SF and 30 m in KF (other variables are calculated from the 2009 along-fjord CTD data). For the thicker PW layer, the same τ_x results in $W < 1$, suggesting less influence of direct wind forcing (although indirect wind forcing such as shelf waves may be important). To reach $W = 1$ for the thicker PW layer, it would take a critical wind speed of 27 m s^{-1} in SF and 23 m s^{-1} in KF. These speeds are reachable during strong piteraqs, suggesting that down-fjord winds could induce fluctuations in the PW/AW interface. *Oltmanns et al.* [2013] find that piteraqs with a mean wind speed of 20 m s^{-1} occur 7–8 times per winter in SF, implying that along-fjord wind is a non-negligible factor for driving exchange in the fjord, on top of its effects in blowing sea ice and icebergs out of the fjord.

The freshwater Froude number, $F_f = U_f/U_d$, quantifies the magnitude of the freshwater forcing on the fjord compared to its stratification. Here $U_f = Q_f/A$, is the barotropic velocity due to freshwater runoff (Q_f) through a cross-sectional area A, and $U_d = (\beta_s gS_0 H)^{1/2}$ is twice the fastest internal gravity wave speed sustained by the observed density field, sometimes called the densimetric velocity [*MacCready and Geyer*, 2010; *Geyer and Ralston*, 2011]. H is the fjord depth and S_0 is the ocean salinity at the fjord mouth. In Greenland's glacial fjords it is difficult to estimate Q_f, but even given a large uncertainty it is clear that $F_f << 1$ in both SF and KF (Table 3). Limiting the depth to above sill level, so $H = H_s$, increases F_f only slightly, highlighting the relatively small runoff values in these fjord systems compared to other factors.

Observed barotropic tidal currents in SF are small (and are expected to be small in KF as well, given the tidal range and fjord depth). Their effect on the estuarine dynamics is quantified through the estuarine Richardson number, Ri_e,

$$Ri_e = \frac{\beta_s gS_0 HU_f}{U_T^3} \quad , \tag{4}$$

where U_T is the tidal current magnitude. Ri_e compares the energy input by the freshwater buoyancy forcing to the dissipation of energy due to bottom drag by tidal currents. $Ri_e > 1$ is an indicator that highly stratified conditions should exist, and indeed, in both SF and KF, $Ri_e >> 1$ (Table 3). The strong stratification and deep depths in these fjords imply that a huge store of potential energy exists. We can quantify this energy storage with the potential energy anomaly, Φ (J m^{-2}),

$$\Phi = g \int (\rho(z) - \rho_0)z \; dz \quad , \tag{5}$$

where the integral is taken over the water column. Φ represents the energy required to mix the entire water column [e.g., *Geyer and Ralston*, 2011]. For SF and KF we calculate Φ based on cross-fjord averages of ρ at each section (Table 3). The range of 6–9 10^5 J m^{-2} is high even for fjords [*Salcedo-Castro et al.*, 2011], underscoring the large amount of energy stored in the stratification. These values are comparable to Φ from Jakobshavn Isbrae [*Burton et al.*, 2012]. *Burton et al.* [2012] used these values of Φ to compare to the mixing energy released by a calving iceberg, suggesting that the entire water column could be mixed by a large

calving event. However, given the fact that no unstratified profiles have ever been observed in SF, KF, or Jakobshavn, the restratification of the water column after such an event would have to take place rapidly, drawing on the large potential energy available in the rest of the fjord and on the shelf.

The overall picture that emerges from characterizing SF and KF in terms of estuarine dynamics is one of a highly stratified system where freshwater forcing and tidal currents are both weak. Indeed, to differentiate these deep-silled glacial fjords in Greenland from one another will take a new parameter space that accounts for more than freshwater input and density-driven exchange flow alone. These additional parameters should include the effect of the intermediary circulation, tidal residual flows, and the potentially strong along-fjord wind forcing. Additional challenges to overcome include the unique features of these fjords—uncertainty in Q_f, how freshwater injected mid-depth alters the estuarine exchange flow, and what controls mixing in the absence of strong tidal currents.

5. Parameterizing Fjord Circulation Regimes

5.1. Intermediary Circulation, Q_i

Given the dominance of the intermediary circulation suggested by the 2009 sections in SF and KF, it would be helpful to be able to predict when, if at all, the intermediary circulation might be important in other fjord systems.

A simple formula for an order of magnitude volume transport estimate due to the intermediary circulation, Q_i, is

$$Q_i = \beta_i [H_s B_m A_f g \Delta M / \rho_0]^{1/2}, \tag{6}$$

where H_s is the sill depth, B_m is the minimum of the mouth width or the local Rossby radius of deformation, A_f is the surface area of the fjord, and ΔM is the vertical integral of the standard deviation of density at the fjord mouth [*Aure et al.*, 1996; *Stigebrandt*, 2012]. Here we calculate ΔM as

$$\Delta M = \int_{-H_s}^{\eta} \sigma_\rho^{1/2}(z)\,dz, \tag{7}$$

where $\sigma_\rho^{1/2}$ is the standard deviation of $\rho(z)$ and the integral is taken only above sill depth to the sea surface, η. The original formulation was based empirically on observations from numerous Norwegian fjords, with $\beta_i = 17 \times 10^{-4}$, a constant found to achieve the best fit [*Stigebrandt*, 2012]. Thus, without other location specific observations from Greenland, we use the same β_i value. Note that calculation of ΔM must be done with special care, as the density variations that matter are only the ones that drive intermediary circulations, i.e., without aliasing low-frequency (interannual or seasonal) and high-frequency (e.g., tidal) fluctuations into the calculated variance. An alternative formulation for the exchange due to the intermediary circulation, termed "baroclinic pumping," requires more data, such as time series of interface depth [*Arneborg*, 2004].

To calculate ΔM for SF, density profiles are taken from the mouth and the two offshore sections, while only the mouth section is used for KF. To ensure that the 2009 data were not anomalous, we calculate ΔM using two additional years of CTD profiles taken at the mouth of SF in 2008 and 2011 (the 2008 data are discussed in *Straneo et al.* [2010], while the 2011 data are unpublished). ΔM ranges from 34 to 51 kg m^{-2} in SF and $\Delta M = 29$ kg m^{-2} in KF in 2009 (Table 4). These values are consistent with point values of $\sigma_\rho^{1/2}$ calculated from a band-passed (excluding fluctuations with time scales > 14 days and < 2 days) time series of density from the moorings S-1 and S-2 for SF. The largest contribution to variability in ΔM comes from $\sigma_\rho^{1/2}$ values found near the AW/PW interface in SF at $\sim$150 m depth and near $\sim$90 m depth at KF. Combined with the fjord geometry (Table 1), we calculate a mean $Q_i = 8.5 \times 10^4$ m^3 s^{-1} for SF and $Q_i = 6.6 \times 10^4$ m^3 s^{-1} for KF. We compare these theoretical Q_i values to observed Q_i values for each fjord, where we use U_{abs} (excluding the mouth). We assume the intermediary circulation is primarily an in/out flow with mass conserved between the layers above sill height. To get the observed Q_i we subtract out a section mean barotropic

Table 4. Estimates of Intermediary Circulation Transport (Q_i) Based on Theory (Q_i theo, equation (6)) and Observations (Q_i obs), Estuarine Exchange Flow Transport (Q_e) for SF and KF, Using Observed Values and Simple Theory Based on Knudsen (Q_e^{kn}), Hydraulic Control (Q_e^{hc}), and Partially Mixed Estuaries (Q_e^{obs}), and the Ratio of Q_i/Q_e[a]

| | Q_i (10^3 m^3 s^{-1}) | | | Q_e (10^3 m^3 s^{-1}) | | | | |
	ΔM (kg m^{-2})	Q_i theo[b]	Q_i obs.	Q_e^{kn}	Q_e^{hc}	Q_e^{est}	Q_e^{obs}	Q_i/Q_e[c]
SF	34–51	85±6	67 ± 16	1.5	4.0	2.2	5.3	23 (8–60)
KF	29	66	83 ± 53	1.1	1.9	2.8	12	17 (4–100)

[a]See text for details.
[b]Plus/minus ranges for all values are ± one standard error, if multiple estimates exist.
[c]The mean ratio is reported with the full range in parentheses.

velocity, then calculate the volume flux where $U_{abs} > 0$. This is done for sections 3–7 in SF and sections 2–3 for KF (Table 4). The observed values are generally consistent with the theoretical Q_i calculated from equation (6), although the range is much greater, spanning 4.1–8.5 $\times 10^4$ m^3 s^{-1} in SF and 4.5–12 $\times 10^4$ m^3 s^{-1} in KF (Table 4). These values of volume flux forced by the intermediary circulation suggest velocity magnitudes of ~0.1 m s^{-1}, much larger than observed barotropic tidal currents, and we next compare them to what we expect from the estuarine, or glacier-driven, circulation.

5.2. Estuarine Circulation, Q_e

We utilize three separate approaches to estimate a velocity for the expected estuarine circulation driven in each fjord. The first is the classic Knudsen relation [*Knudsen*, 1900; *MacCready and Geyer*, 2010] that assumes a two-layer, steady state system with freshwater discharge entering one closed end and uses the conservation of volume and salt to calculate the layer transport, Q_e^{kn}, in the outgoing upper layer,

$$Q_e^{kn} = Q_f(S_2/\Delta S). \qquad (8)$$

where Q_f is the freshwater input into the fjord, S_2 is the salinity of the lower layer, and ΔS the salinity difference between the two layers. Here we set Q_f equal to Q_{sg}, the subglacial flux. The Knudsen relation is advantageous from an observation perspective, but its assumptions are strict: a steady state system with two distinct layers. Both of these conditions are more than likely violated in SF [e.g., *Jackson et al.*, 2014] and KF, and estimating Q_f is difficult in glacial fjords.

The second approach has been used in fjords with shallow sills or narrow constrictions, where one expects to observe a hydraulic control section [*Stommel and Farmer*, 1953; *Farmer and Freeland*, 1983; *Geyer and Ralston*, 2011]. Given a two-layer system, the layer thicknesses, and the density difference between them, hydraulic theory can be applied to calculate the outgoing volume flux, Q_e^{hc}

$$Q_e^{hc} = \left[\frac{Q_{FW}\beta_s g S_2}{B_m}\right]^{1/3} B_m H_s/2, \qquad (9)$$

where the left hand term in the brackets is the velocity prediction by hydraulic control. To get a volume flux, we multiply by the fjord width and half its depth above sill level—the latter is an approximation, as we observe upper layer depths to be much thinner than lower layer depths in SF and KF.

Finally, the third estimate for Q_e is based on theory derived for partially mixed estuaries. This approach is advantageous as it is based on the dominant physics present in most estuaries and explicitly accounts for mixing and the dynamic length of the system, however its applicability to deep fjords is questionable. *MacCready and Geyer* [2010] show that the volume transport driven by the estuarine exchange circulation, Q_e^{est}

$$Q_e^{est} = \frac{g\beta_s \bar{S}_x H^3}{48K_m} B_m H_s/2, \qquad (10)$$

where H is the total depth of the system, $\bar{S}_x$ is the depth averaged along-estuary salinity gradient, and K_m is

an eddy viscosity that parameterizes the mixing processes balancing the baroclinic pressure gradient that drives the flow. Since tides are weak in these fjords and the bottom is deep, we choose an alternate parameterization for K_m based on the width of the fjords, where $K_m = 0.0035 U_i B_m$, and use the velocity magnitude of the observed intermediary circulation that drives these flows, $U_i = 0.1$ m s^{-1}, with a characteristic length scale set by the fjord width [*Banas et al.*, 2004].

5.3. Comparing Q_i and Q_e

Given the assumptions in each Q_e estimate, none of them is deemed entirely satisfactory for SF or KF. Thus, we use all three to see the range in estimates, plus an additional estimate based on *Sutherland and Straneo* [2012] for SF and the background velocity calculated above for KF. To calculate Q_e^{kn} we use values from the mouth section of each fjord, while for Q_e^{hc} we use values from the mid-fjord sections, and an along-fjord section is used to calculate $\bar{S}_x$ for Q_e^{est}. For SF, we find the mean of these four estimates is $Q_e = 3.3 \times 10^3$ m^3 s^{-1} and for KF, the mean $Q_e = 4.7 \times 10^3$ m^3 s^{-1} (Table 4). Comparing Q_e to the theoretical and observed Q_i shows the significance of the externally forced, shelf-driven flow to these systems, with $Q_i >> Q_e$.

In order to assess whether $Q_i >> Q_e$ is typical of a fjord a priori, one could use existing data to estimate Q_i and Q_e in combination with the fjord geometries listed in Table 1. We expect that deep-silled fjords (i.e., large relative values of H_s/H) will have large Q_i/Q_e ratios, whereas fjords with shallow sills will be more constricted in their exchange with the coastal ocean. In these fjords, the estuarine, buoyancy-driven circulation may be more important, although other processes, such as internal tides or along-fjord winds need to be quantified.

5.4. Implications for Glacier/Ocean Interactions

This study suggests that Greenland fjords with deep sills ($H_s/H > 0.25$) are highly dynamic systems with rapidly changing hydrographic properties. The results presented here from SF and KF support previous studies showing significant temporal variability in temperature, salinity, and velocity fields at all depths inside SF [*Straneo et al.*, 2010; *Jackson et al.*, 2014]. The fjords appear to respond quickly to changes in the adjacent coastal ocean, i.e., the fundamental driver of fjord stratification is the ambient ocean stratification immediately outside each fjord. This stratification modulates the circulation within the fjord, shaping the structure of the intermediary circulation and the export of glacially modified water. Indeed, we find evidence that supports the multicellular structure in KF, as inferred by *Straneo et al.* [2011] in SF.

Although we have shown that the intermediary circulation signal masks other flows during synoptic surveys in SF and KF, we are not suggesting that the estuarine circulation is unimportant in these fjords. Indeed, the net freshwater input into the fjords must drive a net circulation that is amplified by entrainment at the glacier face and along the plume's path(s) out of the fjord. The intermediary circulation over the long term will not drive a net, vertically integrated transport in the fjord. What are unclear are the relative magnitudes of heat transport toward the glacier face due to the intermediary circulation versus the estuarine circulation. For the estuarine circulation, the calculation is simpler in theory, but difficult in practice because of the signal being masked by the stronger and time-varying Q_i. To calculate the heat transport due to Q_i, one needs simultaneous measurements of temperature, with the mean and estuarine signals removed. That is, we need to calculate $\overline{Q_i T_i}$, where the overbar is an average over the synoptic scale, and T_i is the temperature band-passed over intermediary circulation frequencies. This term is likely nonzero, but its magnitude compared to the advective flux of heat due to the estuarine exchange flow is unknown. Moored measurements from SF during nonsummer months [September to May] could not extract a meaningful net heat transport due to the intermediary circulation [*Jackson et al.*, 2014]. We do know, however, that Q_i should increase in winter due to stronger winds, while Q_e should decrease as freshwater input decreases seasonally. Thus, the relative magnitudes of Q_i and Q_e, both in terms of volume and heat transport, are expected to change over the year—though the 2009 data for SF and KF indicate that $Q_i >> Q_e$ even in summer. Our results suggest that the volume and heat transport estimates based on synoptic data will be highly variable and not necessarily representative of the mean transport to the glacier. In addition, incomplete velocity measurements cannot be easily extrapolated using simple closures such as geostrophy or estuarine circulation, since our observations indicate that these do not necessarily hold (supporting information, Figures S6–S10). This may help explain the order of magnitude difference in melt rates estimated recently for KF and SF [*Inall et al.*,

2014]. Variations up to 50% of the total magnitude were estimated for submarine melt rates using time series data in SF [*Jackson et al.*, 2014].

Compounding these issues are the unknown feedbacks between Q_i and Q_e. The estuarine circulation depends on $\bar{S}_x$, which can be altered by mixing induced by the intermediary circulation. Also, the layered structure of the estuarine flow in these fjords implies that part of the outflow is occurring at the interface between the PW/AW layers, potentially affecting Q_i, which is driven by changes in this interface depth.

One might choose outlet glacier fjords to study based on predictions of Q_i/Q_e to explore the parameter space of fjord circulation in Greenland. The fact that SF and KF exhibit these highly dynamic flows is important, but significant variability in glacier speeds and thickness exists across regional and local scales in over 200 outlet glacier systems [e.g., *Moon et al.*, 2012]. It would be interesting to test how much of this variability can be linked to fundamental differences in fjord circulation.

6. Conclusions

The summer 2009 data presented here for Sermilik Fjord and Kangerdlugssuaq Fjord are the most highly resolved hydrographic and velocity surveys to date of large, Greenlandic outlet glacier/fjord systems. In both fjords, we find evidence for the intermediary circulation superimposed on a weaker background flow, assumed to be the buoyancy-driven estuarine exchange flow. This buoyancy-driven flow has a similar structure in both fjords, with two regions of outflow (at the surface and at the pycnocline) that make it difficult to apply classic estuarine theory developed for simpler two-layer systems not receiving subsurface freshwater discharge.

At the fjord mouths and immediately offshore, we find that large-scale geostrophic dynamics are more important. The subpolar gyre circulation controls the flows observed here and directly modulates the intermediary circulation inside each fjord mouth. The snapshots of volume and freshwater transport calculated from the 2009 data here suggest that these fjords may have a greater impact on the coastal circulation than previously thought, as they amplify the freshwater input before exporting it to the shelf.

We have put the results from KF and SF in context with other fjord/glacier systems by comparing the relative magnitudes of the estuarine circulation and the intermediary circulation based on simple, existing theories. We find that in these deep-silled fjords, the intermediary circulation drives a transport that is an order of magnitude greater than the expected estuarine circulation. In general, these two fjords can be characterized as highly stratified estuaries where freshwater forcing and tidal currents are weak. We expect future work to examine the relative magnitudes of the intermediary circulation and the estuarine circulation in many of the other 200+ outlet glacier systems surrounding the Greenland coast, with the goal to constrain the dominant dynamics a priori.

References

Amundson, J. M., M. Fahnestock, M. Truffer, J. Brown, M. P. Luthi, and R. J. Motyka (2010), Ice mélange dynamics and implications for terminus stability, Jakobshavn Isbrae, Greenland, *J. Geophys. Res.*, *115*, F01005, doi:10.1029/2009JF001405.

Andersen, M. L., et al. (2010), Spatial and temporal melt variability at Helheim Glacier, East Greenland, and its effect on ice dynamics, *J. Geophys. Res.*, *115*, F04041, doi:10.1029/2010JF001760.

Andrews, J. T., J. D. Milliman, A. E. Jennings, N. Rynes, and J. L. Dwyer (1994), Sediment thicknesses and Holocene glacial marine sedimentation rates in three East Greenland fjords (ca 68°N), *J. Geol.*, *102*(6), 669–683.

Arneborg, L. (2004), Turnover times for the water above sill level in Gullmar Fjord, *Cont. Shelf Res.*, *24*, 443–460, doi:10.1016/j.csr.2003.12.005.

Arneborg, L., and B. Liljebladh (2001), The internal seiches in Gullmar Fjord. Part I: Dynamics, *J. Phys. Oceanogr.*, *31*, 2549–2566.

Aure, J., J. Molvaer, and A. Stigebrandt (1996), Observations of inshore water exchange forced by a fluctuating offshore density field, *Mar. Pollut. Bull.*, *33*, 112–119.

Azetsu-Scott, K., and F. C. Tan (1997), Oxygen isotope studies from Iceland to an East Greenland fjord: Behavior of glacial meltwater plume, *Mar. Chem.*, *56*, 239–251.

Bacon, S., G. Reverdin, I. G. Rigor, and H. M. Smith (2002), A freshwater jet on the east Greenland shelf, *J. Geophys. Res.*, *107*(C7), doi:10.1029/2001JC000935.

Banas, N. S., B. M. Hickey, P. MacCready, and J. A. Newton (2004), Dynamics of Willapa Bay, Washington, a highly unsteady partially mixed estuary, *J. Phys. Oceanogr.*, *34*, 2413–2427.

Brearley, J. A., R. S. Pickart, H. Valdimarsson, S. Jonsson, R. W. Schmitt and T. W. Haine (2012), The East Greenland boundary current system south of Denmark Strait, *Deep Sea Res., Part I*, *63*, 1–19.

Bruce, J. G. (1995), Eddies southwest of the Denmark Streait, *Deep Sea Res., Part I*, *42*, 13–29.

Burton, J. C., J. M. Amundson, D. S. Abbot, A. Boghosian, L. M. Cathles, S. Correa-Legisos, K. N. Darnell, N. Guttenberg, D. M. Holland, and D. R. MacAyeal (2012), Laboratory investigations of iceberg capsize dynamics, energy dissipation, and tsunamigenesis, *J. Geophys. Res.*, *117*, F01007, doi:10.1029/2011JF002055.

Chen, S.-N., and L. P. Sanford (2009), Axial wind effects on stratification and longitudinal salt transport in an idealized partially mixed estuary, *J. Phys. Oceanogr.*, *39*, 1905–1920, doi:10.1175/2009JPO4016.1.

Christoffersen, P., R. I. Mugford, K. J. Heywood, I. Joughin, J. A. Dowdeswell, J. P. M. Syvitski, A. Luckman, and T. J. Benham (2011), Warming of waters in an East Greenland fjord prior to glacier retreat: Mechanisms and connection to large-scale atmospheric conditions, *Cryosphere*, *5*(3), 701–714, doi:10.5194/tc-5-701-2011.

Christoffersen, P., M. O'Leary, J. H. van Angelen, and M. van den Broeke (2012), Partitioning effects fro ocean and atmosphere on the calving stability of Kangerdlugssuaq Glacier, East Greenland, *Ann. Glaciol.*, *53*(60), 249–256, doi:10.3189/2012AoG60A087.

Enderlin, E. M., I. M. Howat, S. Jeong, M.-J. Noh, J. H. van Angelen, M. R. van den Broeke (2014), An improved mass budget for the Greenland ice sheet. *Geophys. Res. Lett.*, *41*, doi:10.1002/2013GL059010.

Farmer, D. M., and H. J. Freeland (1983), The physical oceanography of fjords, *Prog. Oceanogr.*, *12*, 147–220.

Geyer, W. R. (1997), Influence of wind on dynamics and flushing of shallow estuaries, *Estuarine Coastal Shelf. Sci.*, *44*, 713–722.

Geyer, W. R., and G. A. Cannon (1982), Sill processes related to deep water renewal in a fjord, *J. Geophys. Res.*, *87*, 7985–7996.

Geyer, W. R., and D. K. Ralston (2011), The dynamics of strongly stratified estuaries, in *Treatise on Estuarine and Coastal Science*, vol. 2, edited by E. Wolanski and D. McLusky, pp. 37–51, Academic Press, Elsevier, Waltham.

Harden, B. E., I. A. Renfrew, and G. N. Petersen (2011), A climatology of wintertime barrier winds off Southeast Greenland, *J. Clim.*, *24*, 4701–4717.

Hickey, B. M., and N. S. Banas (2003), Oceanography of the U.S. Pacific Northwest coastal ocean and estuaries with application to coastal ecology, *Estuaries*, *28*, 1010–1031.

Holland, D. M., R. H. Thomas, B. De Young, M. H. Ribergaard and B. Lyberth (2008), Acceleration of Jakboshavn Isbræ triggered by warm subsurface ocean waters, *Nat. Geosci.*, *1*, 659–664.

Howat, I. M., B. E. Smith, I. Joughin, and T. A. Scambos (2008), Rates of southeast Greenland ice volume loss from combined ICESat and ASTER observations, *Geophys. Res. Lett.*, *35*, L17505, doi:10.1029/2008GL034496.

Ianniello, J. (1977), Tidally induced residual currents in estuaries of constant breadth and depth, *J. Mar. Res.*, *35*(4), 755–786.

Inall, M. E., T. Murray, F. R. Cottier, K. Scharrer, T. J. Boyd, K. J. Heywood, and S. L. Bevan (2014), Oceanic heat delivery via Kangerdluggsuaq Fjord to the south-east Greenland ice sheet, *J. Geophys. Res. Oceans*, *119*, 631–645, doi:10.1002/2013JC009295.

Jackson, R. H., F. Straneo, and D. A. Sutherland, (2014), Externally forced fluctuations in ocean temperature at Greenland glaciers in nonsummer months, *Nat. Geosci.*, doi:10.1038/ngeo2186, in press.

Jakobsen, P. K., M. H. Ribergaard, D. Quadfasel, T. Schmith, and C. W. Hughes (2003), Near-surface circulation in the northern North Atlantic as inferred from Lagrangian drifters: Variability from the mesoscale to the interannual, *J. Geophys. Res.*, *108*(C8), 3251, doi:10.1029/2002JC001554.

Jakobsson, M., et al. (2012), The International Bathymetric Chart of the Arctic Ocean (IBCAO) Version 3.0, *Geophys. Res. Lett.*, *39*, L12609, doi:10.1029/2012GL052219.

Jenkins, A. (1999), The impact of melting ice on ocean waters, *J. Phys. Oceanogr.*, *29*, 2370–2381.

Jennings, A. E., K. L. Knudsen, M. Hald, C. V. Hansen, and J. T. Andrews (2002), A mid-Holocene shift in Arctic sea-ice variability on the East Greenland shelf, *Holocene*, *12*, 49–58, doi:10.1191/0959683602hl519rp.

Johnson, H. L., A. Munchow, K. Falkner, and H. Melling (2011), Ocean circulation and properties in Petermann Fjord, Greenland, *J. Geophys. Res.*, *116*, C01003, doi:10.1029/2010JC006519.

Kalnay, E., et al. (1996), The NCEP/NCAR 40-year reanalysis project, *Bull. Am. Meteorol. Soc.*, *77*, 437–470.

Klinck, J. M., J. J. O'Brien, and H. Svendsen (1981), A simple model of fjord and coastal circulation interaction, *J. Phys. Oceanogr.*, *11*, 1612–1626.

Knudsen, M. (1900), Ein hydrographischer Lehrsatz, *Ann. Hydrogr. Mar. Meteorol.*, *28*, 316–320.

Large, W. G., and S. Pond (1981), Open ocean momentum flux measurements in moderate to strong winds, *J. Phys. Oceanogr.*, *11*, 324–336.

MacCready, P., and W. R. Geyer (2010), Advances in estuarine physics, *Ann. Rev. Mar. Sci.*, *2*, 141–164, doi:10.1146/annurev-marine-120308-081015.

Magaldi, M. G., T. W. N. Haine, and R. S. Pickart (2011), On the nature and variability of the East Greenland Spill Jet: A case study in summer 2003, *J. Phys. Oceanogr.*, *41*, 2307–2327, doi:10.1175/JPO-D-10-05004.1.

Mernild, S. H., G. E. Liston, and M. van den Broeke (2012), Simulated internal storage buildup, release, and runoff from Greenland Ice Sheet at Kangerlussuaq, West Greenland, *Arct. Antarct. Alp. Res.*, *44*(1), 83–94, doi:10.1657/1938-4246-44.1.83.

Moon, T., I. Joughin, B. Smith, and I. Howat (2012), 21st-Century Evolution of Greenland Outlet Glacier Velocities, *Science*, *336*(6081), 576–578, doi:10.1126/science.1219985.

Mortensen, J., K. Lennert, J. Bendtsen, and S. Rysgaard, (2011), Heat sources for glacial melt in a sub-Arctic fjord (Godthåbsfjord) in contact with the Greenland Ice Sheet, *J. Geophys. Res.*, *116*, C01013, doi:10.1029/2010JC006528.

Motyka, R. J., L. Hunter, K. A. Echelmeyer, and C. Connor (2003), Submarine melting at the terminus of a temperate tidewater glacier, LeConte Glacier, Alaska, USA, *Ann. Glaciol.*, *36*(1), 57–65.

Murray, T., et al. (2010), Ocean-regulation hypothesis for glacier dynamics in south-east Greenland and implications for ice-sheet mass changes, *J. Geophys. Res.*, *115*, F03026, doi:10.1029/2009JF001522.

Nilsen, F., F. Cottier, R. Skogseth, and S. Mattsson (2008), Fjord-shelf exchanges controlled by ice and brine production: The interannual variation of Atlantic Water in Isfjorden, Svalbard, *Cont. Shelf Res.*, *28*, 1838–1853, doi:10.1016/j.csr.2008.04.015.

Oltmanns, M., F. Straneo, G. W. K. Moore, and S. H. Mernild (2013), Strong downslope wind events in Ammassalik, SE Greenland, *J. Clim.*, *27*, 977–993, doi:10.1175/JCLI-D-13-00067.1.

Padman, L., and S. Erofeeva (2004), A barotropic inverse tidal model for the Arctic Ocean, *Geophys. Res. Lett.*, *31*, L02303, doi:10.1029/2003GL019003.

Pawlowicz, R., R. Beardsley, and S. Lentz (2002), Classical tidal harmonic analysis including error estimates in MATLAB using T_TIDE, *Comput. Geosci.*, *28*, 929–937.

Pickart, R. S. (2008), Cruise report: R/V Knorr Cruise KN194 Leg IV, WHOI technical report, 5 pp., Woods Hole Oceanogr. Inst., Woods Hole, Mass. [Available at http://www.whoi.edu/science/PO/pickart/.]

Rignot, E., M. Koppes, and I. Velicogna, (2010), Rapid submarine melting of the calving faces of West Greenland glaciers, *Nat. Geosci.*, *3*, 187–191.

Roberts, D. H., B. R. Rea, T. P. Lane, C. Schnabel, and A. Rodes (2013), New constraints on Greenland ice sheet dynamics during the last glacial cycle: Evidence from the Uummannaq ice stream system, *J. Geophys. Res. Earth Surf.*, *118*, 519–541, doi:10.1002/jgrf.20032.

Rudels, B., E. Fahrbach, J. Meincke, G. Budeus, and P. Eriksson (2002), The East Greenland Current and its contribution to Denmark Strait overflow, *ICES J. Mar. Sci.*, *59*, 1133–1154.

Salcedo-Castro, J., D. Bourgault, and B. deYoung (2011), Circulation induced by subglacial discharge in glacial fjords: Results from idealized numerical simulations, *Cont. Shelf Res.*, *31*, 1396–1406, doi:10.1016/j.csr.2011.06.002.

Schjøth, F., C. S. Andresen, F. Straneo, T. Murray, K. Scharrer, and A. Korablev (2012), Campaign to map the bathymetry of a major Greenland fjord, *Eos Trans. AGU*, *93*(14), 141.

Schumann, K., D. Volker, and W. R. Weinrebe (2012), Acoustic mapping of the Ilulissat ice fjord mouth, west Greenland, *J. Quat. Sci. Rev.*, *40*, 78–88.

Sciascia, R., F. Straneo, C. Cenedese, and P. Heimbach (2013) Seasonal variability of submarine melt rate and circulation in an East Greenland fjord, *J. Geophys. Res. Oceans*, *118*, 2492–2506, doi:10.1002/jgrc.20142.

Stearns, L. A., and G. S. Hamilton (2007), Rapid volume loss from two east Greenland outlet glaciers quantified using repeat stereo satellite imagery, *Geophys. Res. Lett.*, *34*, L05503, doi:10.1029/2006GL028982.

Stigebrandt, A. (1990), On the response of the horizontal mean vertical density distribution in a fjord to low-frequency density fluctuations in the coastal water, *Tellus, Ser. A*, *42*, 605–614.

Stigebrandt, A. (2012), Hydrodynamics and circulation of fjords, in *Encyclopedia of Lakes and Reservoirs*, edited by L. Bengtsson, R. W. Herschy, and R. W. Fairbridge, pp. 327–344, Springer Science, Dordrecht, Netherlands, doi:10.1007/978-1-4020-4410-6.

Straneo, F., G. S. Hamilton, D. A. Sutherland, L. A. Stearns, F. Davidson, M. O. Hammill, G. B. Stenson, and A. Rosing-Asvid (2010), Rapid circulation of warm subtropical waters in a major, East Greenland glacial fjord, *Nat. Geosci.*, *3*, 182–186, doi:10.1038/ngeo764.

Straneo, F., R. G. Curry, D. A. Sutherland, G. S. Hamilton, C. Cenedese, K. Vage, and L. A. Stearns (2011), Impact of fjord dynamics and glacial runoff near Helheim Glacier, *Nat. Geosci.*, *4*, 322–327, doi:10.1038/NGEO1109.

Straneo, F., D. A. Sutherland, D. Holland, C. Gladish, G. Hamilton, H. Johnson, E. Rignot, Y. Xu, and M. Koppes (2012), Characteristics of ocean waters reaching Greenland's glaciers, *Ann. Glaciol.*, *53*(60), 202–210, doi:10.3189/2012AoG60A059.

Sutherland, D. A., and R. S. Pickart (2008), The East Greenland Coastal Current: Structure, variability, and forcing, *Progr. Oceanogr.*, *78*, 58–77, doi:10.1016/j.pocean.2007.09.006.

Sutherland, D. A., and F. Straneo (2012), Estimating ocean heat transport and submarine melt rate in Sermilik Fjord, Greenland, using lowered ADCP profiles, *Ann. Glaciol.*, *53*(60), 50–58, doi:10.3189/2012AoG60A050.

Sutherland, D. A., P. MacCready, N. S. Banas, and L. F. Smedstad (2011), A model study of the Salish Sea estuarine circulation, *J. Phys. Oceanogr.*, *41*, 1125–1143, doi:10.1175/2011JPO4540.1.

Sutherland, D. A., F. Straneo, G. B. Stenson, F. J. M. Davidson, M. O. Hammill, and A. Rosing-Asvid (2013), Atlantic water variability on the SE Greenland continental shelf and its relationship to SST and bathymetry, *J. Geophys. Res. Ocerns*, *118*, 847–855, doi:10.1029/2012JC008354.

Svendsen, H., and R. O. R. Y. Thompson (1978), Wind driven circulation in a fjord, *J. Phys. Oceanogr.*, *8*, 703–712.

Walters, R. A., E. G. Josberger, and C. L. Driedger (1988), Columbia Bay, Alaska: An "upside down" estuary, *Estuarine Coastal Shelf Sci.*, *26*, 607–617.

Winant, C. D. (2008), Three-dimensional residual tidal circulation in an elongated, rotating basin, *J. Phys. Oceanogr.*, *38*, 1278–1295.

Xu, Y., E. Rignot, D. Menemenlis, and M. Koppes (2012), Numerical experiments on subaqueous melting of Greenland tidewater glaciers in response to ocean warming and enhanced subglacial discharge, *Ann. Glaciol.*, *53*(60), 229–234, doi:10.3189/2012AoG60A139.

Yankovsky, A. E., and D. C. Chapman (1997), A simple theory for the fate of buoyant coastal discharges, *J. Phys. Oceanogr.*, *27*, 1386–1401.